The interplay between lysosome, protein corona and biological effects of cationic carbon dots: Role of surface charge titratability

Yasmin Arezki, Ezeddine Harmouch, François Delalande, Mickaël Rapp, Christine Schaeffer-Reiss, Ophélie Galli, Sarah Cianférani, Luc Lebeau, Françoise Pons, Carole Ronzani

The interplay between lysosome, protein corona and biological effects of cationic carbon dots: role of surface charge titratability

Yasmin Arezki [a], Ezeddine Harmouch [a], François Delalande [b,c], Mickaël Rapp [a], Christine Schaeffer-Reiss [b,c], Ophélie Galli [a], Sarah Cianférani [b,c], Luc Lebeau [a], Françoise Pons [a] and Carole Ronzani [a,*]

[a] Laboratoire de Conception et Application de Molécules Bioactives, UMR 7199

CNRS-Université de Strasbourg, Illkirch, France

[b] Laboratoire de Spectrométrie de Masse BioOrganique, IPHC, UMR 7178,

CNRS-Université de Strasbourg, Strasbourg, France

[c] Infrastructure Nationale de Protéomique ProFI – FR2048 CNRS, Strasbourg, France

* Corresponding author at : UMR 7199, Faculté de Pharmacie, 74 route du Rhin, 67400 Illkirch, France.

E-mail address: ronzani@unistra.fr (C. Ronzani).

Abstract

Carbon dots (CDs) are nanoparticles (NPs) with potential applications in the biomedical field. When in contact with biological fluids, most NPs are covered by a protein corona. As well, upon cell entry, most NP are sequestered in the lysosome. However, the interplay between the lysosome, the protein corona and the biological effects of NPs is still poorly understood. In this context, we investigated the role of the lysosome in the toxicological responses evoked by four cationic CDs exhibiting protonatable or non-protonatable amine groups at their surface, and the associated changes in the CD protein corona. The four CDs accumulated in the lysosome and led to lysosomal swelling, loss of lysosomal integrity, cathepsin B activation, NLRP3 inflammasome activation, and cell death by pyroptosis in a human macrophage model, but with a stronger effect for CDs with titratable amino groups. The protein corona formed around CDs in contact with serum partially dissociates under lysosomal conditions with subsequent protein rearrangement, as assessed by quantitative proteomic analysis. The residual protein corona still contained binding proteins, catalytic proteins, and proteins involved in the proteasome, glycolysis, or PI3k-Akt KEGG pathways, but with again a more pronounced effect for CDs with titratable amino groups. These results demonstrate an interplay between lysosome, protein corona and biological effects of cationic NPs in link with the titratability of NP surface charges.

Keywords: Carbon dots, Surface charge, Protein corona, Lysosome, Proton sponge effect, Proteomics

1. Introduction

Over the past decade, carbon-based nanoparticles (NPs) called carbon dots (CDs) have emerged as interesting nanomaterials for widespread applications (Himaja et al., 2015; Truskewycz et al., 2022). CDs are quasi-spherical NPs with exciting properties, including very small size (less than 10 nm), chemical stability, high water solubility, tunable intrinsic fluorescence, and resistance to photobleaching (Xu et al., 2004). They can be easily synthesized, most often by carbonization process of cost-effective organic materials (citric acid, glucose…) in the presence of catalysts and/or passivation reagents. The resulting CDs can be easily chemically functionalized to provide nano-objects with a wide variety of chemical groups at their surface (Huang et al., 2019; Sciortino et al., 2018). In addition to their applications in innovative industrial technologies, such as optoelectronics, photovoltaics or energy storage, CDs are currently being developed in nanomedicine as efficient and versatile nanoplatforms for drug or gene delivery, biomedical imaging and theranostic applications (Claudel et al., 2019; Ghosal and Ghosh, 2019; Pierrat et al., 2015). The safe exploitation of CDs in nanomedicine however requires a deeper understanding of CD interactions with biological systems.

Lysosomes are acidic organelles that play a key role in many biochemical processes including the degradation of extracellular elements and recycling of intracellular metabolic waste (Settembre et al., 2013). Maintaining the integrity and function of lysosomes is thus essential to preserve cellular homeostasis. Various forms of stress can induce damage to the lysosome, including changes in activity of lysosomal enzymes, pH of lysosomes or properties of the lysosomal membrane (Wang et al., 2018). The latter is particularly critical because lysosomal membrane permeabilization induces the release of the organelle content into the cytosol, including protons and proteases such as cathepsin B, leading to mitochondrial dysfunction, activation of the NLRP3 (NOD-like receptor, pyrin domain-containing protein 3) inflammasome and cell death (Kirkegaard and Jaattela, 2009). The implication of the lysosome in the cell death process is complex and involves different pathways such as apoptosis,

necrosis, ferroptosis, necroptosis or pyroptosis (Repnik et al., 2014; Wang et al., 2018). Thus, the lysosome is a particularly sensitive subcellular target that can compromise cell survival.

When therapeutic NPs reach their target cells, they are predominantly internalized by the endocytosis pathway, which involves NP entrapment into an endocytic vesicle, trafficking into the endosomal compartment, and finally accumulation in the lysosome (Canton and Battaglia, 2012; Sahay et al., 2010). If the lysosome is a potential degradation site of NPs, the accumulation of NPs in the lysosomes can trigger dysfunction of the organelle leading to cellular damages and cell death (Stern et al., 2012). Thus, although carbon is not considered as a toxic element, carbon-based nanomaterials have been reported to induce NLRP3 inflammasome activation and cell death due to the disruption of lysosomal homeostasis (Keshavan et al., 2021; Tahara et al., 2012). Concerning CDs, we and others showed that CDs accumulate in lysosomes (Ronzani et al., 2019) and induce lysosome-dependent cell death such as pyroptosis (Arezki et al., 2022b) or necroptosis (Wu et al., 2020). However, the NP lysosomal toxicity is not systematic and could be closely related to the NP characteristics, such as shape (Wang et al., 2018) or surface charge (Weiss et al., 2021), with cationic NPs generally exhibiting greater toxicity than anionic ones (Huhn et al., 2013). Among the mechanisms at the origin of the lysosomal effects induced by cationic NPs, it is suggested that the principle of the “proton sponge” effect may apply. The proton sponge hypothesis was introduced in the 1990s to explain the endo-lysosomal escape properties of cationic macromolecules, e.g., poly(ethyleneimine) (PEI) or chitosan. In the acidic endo-lysosomal compartment, these amine-containing polymers are getting protonated, which induces influx of counter ions inside the compartment, thus provoking the rupture of endosomal membranes due to osmotic swelling (Behr, 1997). Therefore, the incorporation of PEI or polyacids into nanomaterials has been proposed as a tool for improving intracellular delivery of therapeutics by NPs (Faizullin et al., 2022; Li et al., 2021). However, to date, the scientific community has not reached a consensus on the validity of this hypothesis due to contradictory results obtained in various studies (Vermeulen et al., 2018), so that controlling drug delivery after the trafficking of therapeutic NPs inside the endo-lysosomal system still remains a challenge.

On contact with biological fluids, NPs rapidly interact with proteins leading to the formation of the so-called protein corona, which gives NPs a new biological identity and leads to a redefinition of their biological properties (Lynch et al., 2009). Some recent studies have examined the impact of the protein corona on the biological effects of CDs, in the field of food toxicology (Liu et al., 2020; Song et al., 2020) and nanomedicine (Peng et al., 2022). We investigated the relationship between the protein corona, the biological effects and the surface charge of cationic CDs, and found that CDs with high density of cationic charges at their surface are the most highly internalized and toxic to macrophages, in link with the composition of their protein corona (Arezki et al., 2022a). Although these data undoubtedly contribute to a better understanding of the biological effects of CDs, it must be emphasized that most of the targets of NPs developed for biomedical applications, including CDs, are at the subcellular level. But, to date, few studies have focused on the fate and role of the protein corona once the corona-coated NPs become resident in the cells. Yet, it has been suggested that the extracellular protein corona is not stable after NP entering into the cells (Bertoli et al., 2016; Wang et al., 2013b). Indeed, it has been shown that the protein corona is retained on the surface of the NPs upon NP uptake by cells, transported to the lysosomes with the NPs and then degraded in this organelle (Bertoli et al., 2016; Wang et al., 2013b). After passing through the lysosomal compartment, the composition of the protein corona changes qualitatively and quantitatively, and the surface chemistry of the NPs could affect this evolution (Bertoli et al., 2016). Besides, while the protein corona on the surface of the NPs could initially protect the cell from NP-induced damage, a delayed toxicity was observed along with the degradation of the protein corona in lysosomes and the re-exposure of the cells to the toxic surface of the NPs, for cationic polystyrene (Tan et al., 2020; Wang et al., 2013b) or gold (Ma et al., 2015) NPs. In addition, it has recently been observed that, after dissociation of some of the proteins from the initial corona inside the lysosomes, some intracellular proteins can also adsorb to the surface of the NPs (Cai et al., 2022; Wang et al., 2021). This intracellular transformation of the protein corona could impact the NP-induced biological responses, by modifying cellular signaling pathways and metabolic processes, leading to changes in cellular homeostasis (Cai et al., 2022). Thus,

the evolution of the NP protein corona after NP entry into the cells seems to be a key process in the cellular responses to NPs. Understanding this complexity of the nano-bio interface is crucial to better maximizing the biological benefits while minimizing the toxicological risks of therapeutic NPs. However, to the best of our knowledge, the evolution of the CD protein corona after CD cell uptake and trafficking to lysosomes, and how this affects the cytotoxicity of CDs, has not been investigated in the literature yet.

In this context, herein we investigated the interplay between the lysosome, the protein corona and the biological effects of CDs. We focused on polyamine surface-passivated cationic CDs, which are one type of CDs currently developed for gene delivery and theranostic applications (Du et al., 2019). In the present work, 4 CDs were produced from citric acid in the presence of high or low molecular weight branched PEI (MW = 25 kDa, bPEI25k; MW = 600 Da, bPEI600, respectively). Post-functionalization of theses NPs yielded CDs with protonatable (titratable) or non-protonatable (non-titratable) amine groups at their periphery, over a pH range from lysosomal (4.5) to physiological (7.4) pH, in order to identify specific pH effects in the acidic lysosome. Indeed, if our previous data have shown an effect of the ζ-potential and the surface charge density in the CD toxicity (Arezki et al., 2021; Weiss et al., 2021), to what extent a modification of the NP surface charge, induced by lysosomal pH variations, can also influence the NP toxicity had, to our knowledge, never been explored. Thus, the present work aimed to use pH-driven protonatation of amino groups on the surface of CDs as a tool to better understand the role of the lysosome, and in particular the “proton sponge” effect, in the toxicological effects of CDs. As macrophages are one of the main target cells of NPs in the body (Nakayama, 2018), this work was performed on phorbol 12-myristate 13-acetate (PMA)-differentiated THP-1 cells, that represent a suitable model for studying macrophage functions in vitro (Chanput et al., 2014). Besides, in order to investigate the impact of the lysosomal environment on the fate of the NP protein corona, the protein corona formed around these titratable or non-titratable CDs when in contact with serum was characterized, as well as changes in this corona when placed in an artificial lysosomal fluid (ALF). Proteins were quantified by label-free MS-based quantitative proteomics, and

physicochemical properties and biological functions of the identified proteins were analyzed with regards to the titratability of CD surface charge.

2. Material and methods

2.1. Synthesis of CDs

The CDs were prepared according to the following procedures.

CD-PEI25k-T. Citric acid (2.0 g), bPEI25k (8.0 g) and ultrapure water (70 mL) were mixed in a beaker, and pH was adjusted down to 7.0 with 12 N HCl. The colorless resulting solution was heated at 230-250°C under continuous stirring until a brown viscous caramel was formed. The reaction mixture was cooled to rt, diluted with ultrapure water (35 mL), and loaded into a dialysis bag (MWCO 14 kDa) for equilibration against 0.1 N HCl for 96 h, and ultra-pure water for 24 h. The dialysate was filtered through a 0.22 µm PES membrane and freeze-dried to yield of CD-PEI25k-T (2.6 g) as a brown hygroscopic fluffy powder.

CD-PEI600-T. Citric acid (2.0 g), bPEI600 (8.0 g) and ultrapure water (50 mL) were mixed in a beaker, and heated at 160-170°C under continuous stirring. Small portions of water (5 mL) were periodically added to the mixture to prevent vulcanization of the material and immobilization of the magnetic stirring bar. The sticky orange residue was dissolved in HCl 0.1 N, and loaded into a dialysis bag (MWCO 1000 Da) for equilibration against 0.1 N HCl for 24 h, and ultra-pure water for another 24-h period. The dialysate was filtered through a 0.22 µm PES membrane and freeze-dried to yield CD-PEI600-T (1.6 g) as an orange hygroscopic powder.

CD-PEI25k-NT. CD-PEI25k-T (0.50 g) was dissolved in ultrapure water (25 mL), and dimethyl sulfate (5.0 mL) was added under vigorous stirring at room temperature. The biphasic solution was maintained at pH 9-10 by periodic addition of powdered K_2CO_3. After 48 h, the mixture turned homogeneous. Ammonia solution (35 %, 4.0 mL) was added and the resulting mixture was stirred for 1 h more. It was then brought down to pH 2 with 12 N HCl, and dialyzed (MWCO: 1000 Da) against 0.2

N NH_4Cl for 2 h, and ultrapure water for 8 h. To push anion exchange to completion (i.e., sulfate vs. chloride), trimethylamine hydrochloride (0.60 g) was added into the dialysis bag and dialysis was continued for an additional period of 24 h. The dialysate was then filtered through a 0.22 µm PES membrane and freeze-dried to yield CD-PEI25k-NT (0.54 g) as an orange hygroscopic powder.

CD-PEI600-NT. CD-PEI600-NT (0.29 g) was obtained starting from CD-PEI600-T (0.50 g), following the same protocol as for CD-PEI25k-NT.

2.2. Characterization of CDs

All measurements were carried out on fresh CD suspensions (1.0 mg/mL in 1.5 mM NaCl pH 7.4). The hydrodynamic diameter (D) and zeta -potential (ζ) of CDs were determined by dynamic light scattering (DLS) using a Zetasizer Nano ZS apparatus (Malvern Instruments, France). Measurements were carried out in triplicate at 25 °C and data were expressed as mean (± SD). The surface charge density of CDs was determined by polyelectrolyte titration, monitoring ζ variation of CD suspension, along spiking with a solution of poly(acrylic acid) (PAA, MW ± 1,800 Da, NaCl 1.5 mM pH 7.4), as previously described (Weiss et al., 2021). The results were expressed in µmol/mg. The surface charge titratability was determined as the sensitivity of the ionization state of the CDs to the pH of the milieu. It was calculated from titration curves. For that, CD solutions (1.0 mg/mL) at pH 2.4 were added with successive aliquots (10 µL) of 0.1 N NaOH until pH reached the value of 12.0 or more. Titratability of the CDs was specifically considered in the pH range between 4.5 and 7.4 that covers pH values met in the extracellular medium and the various intracellular compartments. It was expressed in µmol/mg and corresponds to the amount of amine groups at the surface of the CDs that are titratable, i.e., that can be protonated or deprotonated, in the pH range considered. Optical properties of CDs were determined by recording UV-visible and fluorescence spectra on CD preparations, using a multimode reader (Varioskan Lux, Thermo Fisher Scientific, France). Fluorescence quantum yields (F) were determined using quinine sulfate as standard, according to a previous report (Pierrat et al., 2015).

2.3. Cell culture

THP-1 cells (TIB-202™, ATCC) were grown at 37 °C in a 5 % CO_2 humidified chamber using RPMI-1640 culture medium containing L-glutamine (2 mM), 2-mercaptoethanol (0.05 mM), penicillin (100 UI/mL), streptomycin (100 µg/ml), and heat inactivated FBS (10 %) (all reagents from GIBCO, France). For experiments, cells were seeded in appropriate culture devices (as described above) and differentiated into macrophages overnight by adding 10 ng/mL of PMA (Sigma-Aldrich, MO, USA) to the culture medium. The expression of surface markers such as CD11b (CR3), CD14 and CD36 was checked by FACS (data not shown), attesting to transition of the cells from a monocyte to a macrophage phenotype (Chanput et al., 2014).

2.4. Assessment of CD trafficking to lysosomes

Confocal laser scanning microscopy (CLSM) was used to assess CD trafficking to lysosomes thanks to the intrinsic fluorescence properties of the NPs. Cells were seeded into 8-well IbiTreat µ-slides (1.5 polymer coverslip, IBIDI®, Ibidi GmbH, Germany) at a density of 1.10^5 cells per well, differentiated into macrophages, and incubated with CDs at a concentration of 12.5 µg/mL for 4 h. At the end of the incubation time, the cells were washed with PBS and exposed to the fluorescent probe LysoTracker® Red DND-99 (50 nM, 30 min, Molecular Probes) in order to label the lysosomes. After washing the cells, the colocalization of CDs with the lysosomes was observed using a Leica SP2 microscope equipped with a 63X oil immersion objective (NA = 1.2). The CDs and the lysosome probe were excited with 405 and 561 nm laser sources, respectively. Quantitative analysis of fluorescence signals associated with CDs and lysosomes was determined as previously described (Ronzani et al., 2019). Briefly, the positions of lysosomes and CDs were obtained for individual image, and the position list obtained for a specific channel was then used to determine the presence or the absence of the other color. By applying this method, a colocation trace (color 1 vs. color 2) could be generated from which the degree of colocalization was obtained by determining a Pearson correlation coefficient (r).

2.5. Lysosomal integrity

Lysosomal integrity was assessed by the neutral red assay. Cells were seeded into 96-well plates at a density of 1.10^5 cells per well, differentiated into macrophages and incubated for 24 h with increasing concentrations of CDs (3–100 µg/mL). The cells were then washed with PBS and incubated with 200 µL of neutral red solution (100 µg/mL in culture medium) for 3 h at 37 °C. At the end of the incubation period, the cell supernatant was removed and the cells were washed with PBS before addition of an extraction solution (200 µL of 1:1 water-ethanol solution containing 1 % acetic acid) for 20 min. Absorbance of the resulting samples was measure at 540 nm. Results were expressed as the percentage of the absorbance of CD-treated cells relative to that of the control unexposed cells.

2.6. Lysosomal swelling

Lysosomal swelling was assessed by fluorescence activated cell sorting (FACS) using the lysosomal marker LysoTracker® Red DND-99. Cells were seeded into 24-well plates at a density of 5.10^5 cells per well, differentiated into macrophages and incubated with 25 µg/mL of CDs for 24 h. After CD exposure, the cells were washed with PBS and incubated with 50 nM LysoTracker in serum-free culture medium for 30 min at 37 °C. At the end of the incubation, the cells were rinsed with PBS, harvested by trypsin treatment, centrifuged and resuspended in serum-free culture medium. Cell suspensions were then analyzed with a LSRFortessa X-20™ flow cytometer (BD Biosciences, France) and sample fluorescence (20,000 events) was analyzed with excitation at 561 nm and signal detection at 586 nm (yellow-green laser, PE channel). Lysosomal swelling was quantified by determining changes in the mean fluorescence intensity (MFI) of CD-treated cells relative to that of untreated cells, as previously described in the literature (Wang et al., 2013a; Wang et al., 2013b). Results were expressed as the ratio of the MFI of CD-treated cells to that of untreated cells.

2.7. Cathepsin B activity

The activity of cathepsin B was quantified by fluorimetry using the Magic Red® assay (CliniSciences, France). Cells were seeded into 96-well plates at a density of 1.10^5 cells per well, differentiated into macrophages and incubated with 25 or 100 µg/mL of CDs for 4 h. After CD exposure, the cells were washed with PBS and incubated with the cathepsin B substrate for 1 h at 37 °C. At the end of the incubation, the cells were washed with PBS, and the sample fluorescence was measured at 590 nm, with excitation at 540 nm. Results were expressed as the ratio of fluorescence intensity measured in cells exposed to CDs to that measured in untreated cells.

2.8. IL-1β secretion assay

For IL-1β secretion assay, cells were seeded into 96-well plates at a density of 1.10^5 cells per well, differentiated into macrophages and incubated or not with a cathepsin B inhibitor (CA-074Me, 10 µM, Enzo life) for 1 h 30, prior to CD exposure (25 or 100 µg/mL) for 24 h. IL-1β was quantified in the supernatant by ELISA (R&D Systems, France), according to the manufacturer's instructions. Absorbance was read at 450 nm with a correction at 570 nm. Cytokine concentrations were expressed in pg/mL.

2.9. Cell viability

Cell viability was assessed by the MTT assay. Cells were seeded into 96-well plates at a density of 1.10^5 cells per well, differentiated into macrophages and incubated for 24 h with increasing concentrations of CDs (3-100 µg/mL). The cells were then washed with PBS and incubated with 100 µL of MTT (1.0 mg/mL, in culture medium) for 1 h at 37 °C. At the end of the incubation, the culture medium was removed, and the cells were lysed with DMSO. Absorbance of the resulting samples was read at 570 nm with a correction at 690 nm. Cell viability was expressed as the percentage of the absorbance of CD-treated cells relative to that of the control untreated cells. To take into account potential interferences between NPs and colorimetric assays such as the MTT test, we carefully washed the cells before adding the MTT solution to remove NPs from the culture. In addition, we

characterized the spectral properties of each CD and verified that the NPs absorbed little or none at the reading wavelength of the MTT assay, i.e., 570 nm (Supplementary Figure S1).

2.10. LDH release

Cells were seeded into 96-well plates at a density of 1.10^5 cells per well, differentiated into macrophages and incubated for 24 h with increasing concentrations of CDs (3-100 µg/mL). After CD exposure, the release of LDH in the culture supernatant was assessed using the Cytotoxicity Detection Kit Plus (Roche Applied Science). LDH activity was measured according to the manufacturer's instructions and expressed as the fold change in absorbance measured in the supernatants of CD-exposed cells relative to that measured in the supernatants of control unexposed cells. We checked that CDs absorbed little or not at the reading wavelength of the LDH assay, i.e., 492 nm (Supplementary Figure S1).

2.11. Pyroptosis cell death mechanism

Pyroptosis was determined by flow cytometry by analyzing the fluorescence signals associated with both the necrosis (propidium iodide, BD Biosciences) and the caspase-1 activity (FAM-FLICA assay, Biorbyt) markers. Cells were seeded into 24-well plates at a density of 5.10^5 cells per well, differentiated into macrophages and incubated with 25 or 100 µg/mL of CDs for 4 h. After CD exposure, the cells were washed with PBS, harvested by trypsin treatment, centrifuged and resuspended in serum-free culture medium (290 µL) containing 10 µL of FAM-FLICA® reagent (1/5 dilution). After a 1-h incubation, each sample was washed with the assay kit buffer, before addition of propidium iodide (1/100 dilution) and fluorescence analysis (20,000 events per sample) with a LSRFortessa X 20™ flow cytometer (BD Biosciences, France), using the FITC (λ_{ex}: 488 nm, λ_{em}: 530 nm, FAM-FLICA®) and PE Texas Red (λ_{ex}: 561 nm, λ_{em}: 610 nm, propidium iodide) channels. Pyroptosis was expressed as the percentage of double-positive cells.

2.12. Preparation of corona samples

Initial corona. The initial corona samples were prepared according to a protocol described elsewhere (Arezki et al., 2022a). Briefly, CD water suspensions (2.0 mg/mL, 250 µL) were sonicated in a sonication bath (40 Hz, for 3 min) and mixed with undiluted FBS (40 mg/mL of protein, 250 µL, GIBCO, France) in Eppendorf® Protein Lobind tubes. The tubes were incubated for 1 h at 37 °C under rocking agitation (70 oscillations per min). The samples were then centrifuged at 14,000 g and 20 °C for 45 min. Supernatants were discarded and the pellets containing the CD-protein complexes were resuspended in ultra-pure water and centrifuged again (14,000 g for 45 min at 20 °C) to remove unbound proteins. The process was repeated twice. The final pellets were resuspended in 100 µL of ultrapure water (initial corona samples) or in 1 mL of ALF (post ALF corona sample preparation, see below).

Post ALF corona. The ALF solution was prepared according to protocols previously described (Beeston et al., 2010; Milosevic et al., 2019). Briefly, sodium chloride (3.210 g), sodium hydroxide (6.000 g), citric acid (20.800 g), calcium chloride (0.097 g), sodium dihydrogen phosphate (0.071 g), sodium sulfate (0.039 g), magnesium chloride hexahydrate (0.106 g), glycerin (0.059 g), sodium citrate dihydrate (0.077 g), sodium tartrate dihydrate (0.090 g), sodium lactate (0.085 g), and sodium pyruvate (0.086 g) were dissolved in 1 L of ultrapure water, and the pH was adjusted to 4.5. CDs with their initial corona were resuspended in 1 mL of ALF, mixed and incubated for 4 h at 37 °C under orbital agitation (850 rpm for 30 min, then 450 rpm for 3 h 30). Based on the literature (Rabel et al., 2021) and preliminary tests, the incubation time in ALF was set at 4 h to allow stabilization of the protein dissociation process from the initial corona. The samples were then centrifuged at 14,000 g and 20 °C for 45 min. Supernatant was discarded and the pellets containing the post ALF corona were resuspended in 100 µL of ultrapure water.

2.13. Qualitative analysis of corona samples by SDS-PAGE

Qualitative analysis of the proteins in the corona samples was performed by SDS polyacrylamide gel electrophoresis (SDS-PAGE). Twenty µL of the samples were mixed with 20 µL of

Laemmli buffer (125 mM Tris-HCl, 4 % SDS, 20 % glycerol, 0.1 % bromophenol, pH 6.8) containing 10 % β-mercaptoethanol. Afterwards, the samples were heated for 5 min at 100 °C, and then 30 µL of the sample or 5 µL of a protein standard (Amersham™ High Range Rainbow Marker, Merck, Germany) were dispensed into the wells of an SDS-PAGE gel (Mini-PROTEAN TGX Precast at 4-15 %, Bio-Rad). Electrophoresis was performed at 160 V, 70 mA for approximately 45 min. The gels were stained for 10 min with Coomassie Brilliant Blue R-250 (Bio-Rad) and destained for 2 h in a solution of ethanol (25 %), acetic acid (10 %) and ultrapure water (65 %). The stained bands were visualized using the FastGene GelPic LED Box imaging system (Nippon Genetics Europe, Germany).

2.14. Protein quantification in corona samples

Proteins were quantified in the corona samples using the BCA method (bicinchoninic acid assay, Sigma-Aldrich, MO, USA). Briefly, 20 µL of sample or standard (freshly prepared bovine serum albumin (BSA) solutions) were placed in the wells of a titration plate. Freshly prepared BCA reagent was added to each well (200 µL) and the plates were incubated at 37 °C for 30 min. Absorbance of the samples at 570 nm was then measured. Protein concentrations were calculated from the calibration curve obtained with BSA.

2.15. Protein corona characterization by proteomic analysis

The initial and post ALF coronas were characterized according to a protocol we have previously described (Arezki et al., 2022a). Briefly, for each sample, 7.5 µg of protein lysate was concentrated on a stacking gel by electrophoresis. The gel bands were cut, washed with ammonium hydrogen carbonate and acetonitrile, reduced, and alkylated before trypsin digestion (Promega). The generated peptides were analyzed on a nanoAcquity UPLC device (Waters, MA, USA) coupled to a Q-Exactive Plus mass spectrometer (Thermo Fisher Scientific, France). A Top 10 method was used with automatic switching between MS and MS/MS modes to acquire high resolution MS/MS spectra. Raw mass spectrometry (MS) data processing was performed using the MaxQuant software v1.6.7.0.86. Peak

lists were searched against a target-decoy database including Bos Taurus protein sequences extracted from Uniprot. False-discovery rates set to 1 % for both peptide spectrum and proteins matches. The LFQ (label-free quantification) and the “match between runs” options were not used. All other MaxQuant parameters were set as default. To be considered, proteins must be identified in all four replicates of at least one condition. To determine the relative abundance for each protein and classify them, we determined the relative intensity-based absolute quantification (riBAQ) for each protein (Lenz and Dihazi, 2016). Then, a cut-off was applied to select only proteins present in all four replicates, and with a riBAQ > 0.05. The mass spectrometry proteomics data have been deposited to the ProteomeXchange Consortium via the PRIDE partner repository (Perez-Riverol et al., 2022) with the dataset identifier PXD042143. The physicochemical properties of the proteins were calculated based on their sequences. The molecular weight (MW) and isoelectric point (pI) were computed via https://isoelectric.org/index.html and the GRAVY index via https://www.bioinformatics.org/sms2/protein_gravy.html. The biological functions of the proteins were analyzed according to the molecular functions and the involvement in KEGG pathway using the classification generated from the DAVID (v 6.8), STRING (v 11.5) and Panther (v 16.0) systems.

2.16. Statistical analysis

Data were expressed as mean ± SEM. Statistical differences between groups were determined by a one- or two-way analysis of variance (ANOVA) followed by a Tukey’s or Sidak’s test, using the GraphPad Prism 6.0 software. Data were considered as significantly different when p value was less than 0.05.

3. Results and discussion

3.1. Design and characterization of CDs

The CDs investigated herein were designed to be cationic and to exhibit protonatable (titratable) or non-protonatable (non-titratable) amine groups at their periphery, over a pH range from lysosomal (4.5) to cytoplasmic pH (7.4). Two different polyamine-based passivating reagents (bPEI25k and bPEI600) were used to obtain titratable CDs (CD-T), namely CD-PEI25k-T and CD-PEI600-T, with primary, secondary and tertiary amine functions on their surface. A post-functionalization step was then realized to obtain the respective non-titratable CDs (CD-NT), namely CD-PEI25k-NT and CD-PEI600-NT, with tetraalkylammonium functions on their surface. The size (D), zeta-potential (ζ), surface charge density (electrokinetic charge, Q_{ek}), surface charge titratability (Q_t) and optical properties of these 4 CDs are presented in Table 1. The mean hydrodynamic diameter of the CDs, determined by DLS, ranged from 9.9 to 15.8 nm, which corresponds to the size generally described in the literature for CDs (Truskewycz et al., 2022). The surface charge and surface charge density of the 4 CDs, measured at pH 7.4, were close to each other, with a ζ-potential greater than +30 mV (ζ from +31.8 to +39.0 mV) and a marked Q_{ek} (from 4.70 to 6.67 µmol/mg). As expected, the CDs differed in their charge titratability. CD-PEI25k-T displayed a large amount of titratable amine groups (Q_t = 3.94 µmol/mg, between pH 4.5 and pH 7.4), while CD-PEI25k-NT had much fewer (Q_t = 0.63 µmol/mg) as most amine groups had been quaternarized. Similarly, CD-PEI600-T had a higher amount of titratable positive charges (Q_t = 3.12 µmol/mg) than CD-PEI600-NT (Q_t = 1.42 µmol/mg). Noteworthy, full quaternarization of all amines at the surface of the CDs is difficult and could not be achieved under the experimental conditions used herein. Nevertheless, the titratability of bPEI25k-based CDs (CD-PEI25k-T vs CD-PEI25k-NT) was reduced by ca. 84 %, whereas the titratability of bPEI600-based CDs (CD-PEI600-T vs CD-PEI600-NT) was reduced by 54 %. Regarding the fluorescence properties of the 4 CDs (Fig. S1), the maximum excitation ranged from 345 to 365 nm, while the fluorescence emission wavelength was maximum at 455-460 nm, which is easy to use for in vitro imaging (Table 1). Thus, we produced two pairs of CDs with titratable and non-titratable positive charges whose biological effects and protein corona could be compared.

Table 1 Physicochemical and photophysical characteristics of the CDs investigated herein

	CD-PEI25k-T	**CD-PEI25k-NT**	**CD-PEI600-T**	**CD-PEI600-NT**
Structure	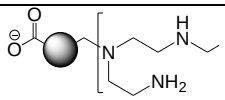	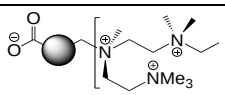	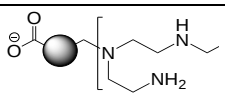	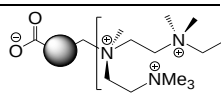
Passivation reagent	bPEI25K	bPEI25K	bPEI600	bPEI600
Hydrodynamic diameter D [nm]	9.9 ± 0.5	15.8 ± 0.9	11.0 ± 3.4	13.2 ± 0.8
Zeta-potential ζ [mV]	+32.4 ± 1.3	+39.0 ± 1.4	+31.8 ± 1.1	+33.3 ± 4.6
Surface charge density Q_{ek} [µmol/mg]	5.52	6.67	4.70	4.78
Surface charge titratability Q_t [µmol/mg]	3.94	0.63	3.12	1.42
Photoluminescence $\lambda_{max}/\lambda_{ex}/\lambda_{em}$ [nm]	[a]/345/460	[a]/360/450	350/365/460	350/360/455

a) Monotonous UV-vis absorption decreasing between 250 and 800 nm.

3.2. Study of CD-T and CD-NT trafficking to the lysosomes

The CD-T and CD-NT trafficking to the lysosomes was investigated in macrophages using CLSM after lysosome staining with the LysoTracker® Red fluorescent probe. As PEI600-based CDs exhibited a higher fluorescence quantum yields than PEI25k-based CDs (F = 12.4 % vs. 1.4 %, respectively), the trafficking of CD-T and CD-NT to the lysosome was studied for the PEI600-based CD pair to facilitate CD intracellular detection and quantitative analysis of lysosomal colocalization with sufficient robustness. It should be noted that a localization of PEI25k-based CDs in lysosomes of macrophages was previously reported by our group (Ronzani et al., 2019), and we assume that this behavior should be maintained in the present study. In the present work, macrophages were exposed to 12.5 µg/mL of CD-PEI600-T or CD-PEI600-NT for 4 h before cell imaging. The concentration of CDs was chosen based on previous work on CD lysosomal trafficking and toxicity (Ronzani et al., 2019). As shown on CLSM pictures (Fig. 1a), the two CDs (blue spots) colocalized with lysosomes (red spots). A quantitative analysis of fluorescence signals associated with CDs and lysosomes (Fig. 1b) confirmed this colocalization for both CD-PEI600-T and CD-PEI600-NT, with positive and statistically significant Pearson's correlation coefficients ($r = 0.45$ with $p < 0.001$ for CD-PEI600-T; $r = 0.30$ with $p < 0.001$ for

CD-PEI600-NT). Thus, our data showed that cationic CDs trafficked into lysosomes after cell uptake, whether they had titratable or non-titratable positive charges on their surface. In the literature, it has already been reported that cationic CDs with amine groups have the ability to target the lysosome (E et al., 2018; Ronzani et al., 2019; Wu et al., 2017). We have further shown here that this intracellular localization is maintained when the amine functions present on the surface of the NPs are less or not sensitive to pH.

3.3. Impact of the titratability of surface charges on the toxicity of CDs

3.3.1. Lysosomal dysfunction induced by CD-T and CD-NT

We assessed whether the accumulation of CDs in the lysosome could lead to a disruption of this organelle. The cells were exposed to increasing concentrations (3-100 µg/mL) of CD-PEI25k and CD-PEI600 with titratable (CD-T) or non-titratable (CD-NT) charges, for 24 h, and the lysosomal integrity was determined using the neutral red assay (Fig. 2a). A dose-dependent loss in lysosomal integrity was observed in response to the 4 CDs, with a significantly stronger effect for CD-T (light grey) compared to CD-NT (dark grey). This loss in lysosomal integrity resulted from lysosomal swelling as showed in cells treated with 25 µg/mL of CDs (Fig. 2b). As the lysosomal protease cathepsin B is one of the main effectors of toxic responses resulting from lysosomal damage (Boya and Kroemer, 2008), cathepsin B activity, as well as the effect of cathepsin B inhibition on CD-induced NLRP3 inflammasome activation, were assessed. As shown in Fig. 2c, CD-PEI25k-T induced a 2.39-fold increase in cathepsin B activity in cells exposed to 25 µg/mL of the NPs for 4 h, whereas CD-PEI25k-NT evoked a 1.45-fold increase in the same conditions. For PEI600-based CDs, only CD-T induced an increase in cathepsin B activity at 25 (1.73-fold) and 100 µg/mL (2.91-fold). As illustrated on Fig. 2d, the IL-1β cytokine, a marker of NLRP3 inflammasome activation, was secreted by macrophages in response to 25 and 100 µg/mL CD-PEI25k and CD-PEI600. This secretion was globally more pronounced for CD-T (white bars) than for CD-NT (grey bars) and was significantly decreased by cathepsin B inhibitor (hatched bars)

for both CD-T or CD-NT. Thus, this showed that cationic CDs induce swelling and loss of membrane integrity of the lysosome in macrophages, leading to the release of cathepsin B, and that this lysosomal dysfunction can lead to subsequent cellular effects such as activation of the NLRP3 inflammasome. In agreement with our data, a link has already been established in the literature between the lysosomal dysfunction induced by carbon-based NPs and NLRP3 inflammasome activation, with a key role for cathepsin B (Svadlakova et al., 2020). Our previous data showed the impact of zeta-potential (Fan et al., 2019) and positive charge density (Weiss et al., 2021) in the lysosomal toxicity of CDs. In the present study, we showed the influence of an additional parameter which is the pH sensitivity of the chemical groups (titratability) at the surface of CDs, as CDs with primary, secondary and tertiary amine groups induced greater lysosomal dysfunction compared to CDs with equivalent non-titratable tetraalkylammonium groups. This point will be discussed below.

3.3.2. Involvement of the lysosome in the cytotoxicity of CD-T and CD-NT

To evaluate the cytotoxicity of CDs on macrophages, the cells were exposed to increasing concentrations of the NPs for 24 h, and the cellular viability was first assessed by measuring cell mitochondrial activity using the MTT assay (Fig. 3a). A dose-dependent decrease in cell viability was observed in response to the PEI25k-based CDs, with a lower EC_{50} value for CD-PEI25k-T compared to CD-PEI25k-NT (17.8 and 28.5 µg/mL, respectively). This loss of cell viability was associated with an increase in the LDH necrosis marker in the culture supernatants of cells exposed to the 2 CDs, but this increase was statistically significant from 12 µg/mL for CD-PEI25k-T and 25 µg/mL for CD-PEI25k-NT (Fig. 3b). The results obtained for PEI600-based CDs also showed more pronounced cytotoxic effects for CD-T (EC_{50} = 19.6 µg/mL and LDH increase from 12 µg/mL), compared to CD-NT (EC_{50} = 103.1 µg/mL and LDH increase from 100 µg/mL). To note that a flow cytometry approach with the Annexin V/propidium iodide assay (data not shown) confirmed the data obtained with the MTT and LDH tests, dispelling any doubt about a possible interference of CDs with these colorimetric tests. We also observed that PEI25k-based CDs induced more cytotoxic effects than PEI600-based CDs. This can be

explained by the nature of the passivation agent used in the CD synthesis (chain length of PEI25k > chain length of PEI600), which governs the quantity of amino groups at the periphery of the CDs, and by the way the surface charge density of the CDs (Q_{ek} of CD-PEI25k > Q_{ek} of CD-PEI600). As we have shown previously (Fan et al., 2019; Weiss et al., 2021), the longer the chain of the amine-based passivation agent, the higher the toxicity of the particles (Fan et al., 2019). In terms of NP characteristics, this translates into a cytotoxicity that dependents on the CD surface charge density (Weiss et al., 2021), which is the case in the present study. In macrophages, the NLRP3 inflammasome activation leading to cell death by pyroptosis via the cleavage and the activation of caspase-1 is a possible consequence of lysosomal dysfunction (Wang et al., 2018). In order to investigate whether the 4 CDs investigated herein could induce macrophage cell death by pyroptosis, the cells exposed to CDs (25 and 100 µg/mL) for 4 h were labelled with the FAM-FLICA and propidium iodide reagents, to measure caspase-1 activity and membrane integrity loss, respectively. The double positive cells were then identified as pyroptotic cells by flow cytometry, as illustrated for the dose of 25 µg/mL of CDs on Fig. 3c. Whereas nearly 80 % of cells exposed to CD-PEI25k-T (25 and 100 µg/mL) and nearly 60 % of cells exposed to CD-PEI600-T (100 µg/mL) were double positive, suggesting macrophage death by pyroptosis, there were globally fewer pyroptotic cells in response to CD-NT (Fig. 3d). Collectively, these results demonstrated that cationic CDs accumulate in the lysosome, leading to lysosomal swelling, loss of lysosomal integrity, cathepsin B activation, NLRP3 inflammasome activation, and ultimately cell death by pyroptosis. Consistent with our data, pyroptosis has recently been incriminated in the toxicity of carbon NPs, notably carbon black NPs (Reisetter et al., 2011) or carbon nanotubes (Wang et al., 2020). Regarding CDs, we have previously shown that cationic CDs with a high density of positive charges at their surface induce inflammasome-dependent pyroptosis in macrophages via lysosomal dysfunction (Arezki et al., 2022b). In the present study, we further demonstrated the influence of the titratability of the positive surface charges, since all the effects observed were stronger for CD-T than for CD-NT. Very few studies have focused on the role of the titratability of the surface charge of NPs on their toxicity. Our data are in agreement with those of Xia et al. who reported an increased

lysosomal toxicity of polystyrene NPs bearing titratable amine groups on their surface compared with those bearing amidine groups (Xia et al., 2008), as amidines are more readily ionized (pKa = 11-12), i.e., less titratable in the pH range considered, than amines (pKa = 9.5-11). Thus, our data support the hypothesis that the "proton sponge" effect is involved in the cellular response to cationic CDs. Indeed, due to the titratable chemical groups at their surface, CD-T can buffer the interior of the lysosome. This may result in an increased accumulation of protons in the compartment associated with an influx of chloride anions and water molecules, leading to osmotic swelling and destabilization/permeabilization of the lysosomal membrane. Recent work did envisage taking advantage of this pH sensitivity of cationic CDs in therapeutic approaches, particularly for the targeted-delivery of anti-cancer drugs inside tumors, whose microenvironment is often acidic due to the Warburg effect (Feng et al., 2016; Lee et al., 2022). However, the nature of the cationic charges present on the surface of therapeutic NPs is still rarely studied, although achieving effective endo-lysosomal release of NPs by the use of proton-sponge effect depends on a delicate balance between proton accumulation in the lysosomal compartment, osmotic swelling and destabilization of the endo-lysosomal membrane (Vermeulen et al., 2018). In fact, our data showed that it may be possible to modulate NP lysosomal effects by the design of NPs with variable amounts of titratable positive charges on their surface. It will be an interesting area for further research, particularly to better control the delivery of drugs carried by therapeutic NPs.

3.4. Impact of the lysosome on the fate of the CD-T and CD-NT protein coronas

3.4.1. Qualitative changes in CD-T and CD-NT protein coronas under lysosomal conditions

It is now well known that the cellular effects of NPs do not only depend on their molecular identity, but that the protein corona also plays a crucial role (Ding et al., 2018). It has been suggested that during cell uptake of NPs, the protein corona is retained on the surface of NPs, trafficked to lysosomes together with the NPs and afterwards degraded inside this organelle (Bertoli et al., 2016;

Wang et al., 2013b). Although recent studies, including our work (Arezki et al., 2022a), have looked at the impact of the protein corona on the cellular uptake of CDs, the evolution of the CD protein corona during trafficking to the lysosomal compartment has never been reported. To address this point in the present study, the 4 CDs were incubated with serum (1 h, 37 °C) according to a protocol previously described (Arezki et al., 2022a), in order to cover them with a protein corona, called "initial corona". The CD-protein complexes were then placed in ALF for 4 h to simulate the lysosomal environment, and then re-isolated to characterize the "post ALF" corona. With a composition, salt concentration and pH value similar to the physiological situation, ALF was proposed several years ago as a simulated lysosomal fluid to assess the degradation of metal NPs in the lysosome (Arbab et al., 2005; Milosevic et al., 2017; Rabel et al., 2019). More recently, some authors used ALF to investigate the evolution of iron oxide NP coronas in the lysosome (Rabel et al., 2021; Stepien et al., 2018). Here, the initial and post ALF coronas were first characterized by SDS-PAGE analysis (Fig. 4a) and quantification of bound proteins was realized by BCA assay (Fig. 4b). A large amount of protein bands was detected by SDS-PAGE analysis in the initial corona of the 4 CDs (molecular weight ranging from 12 to 225 kDa), showing the binding of the most abundant proteins. The observed protein binding pattern was consistent with the SDS-gel protein profile previously described in the literature for lipid-mimicking chlorophyll-based CD protein corona (Peng et al., 2022). Remarkably, protein pattern was changed in the post ALF corona of the 4 CDs, with globally less proteins absorbed compared to the respective initial corona. The results of the BCA assay confirmed these observations with a significant reduction of the quantity of adsorbed proteins after incubation of CD-protein complexes in ALF for all CDs. Indeed, after a 4-h incubation in ALF, only 7-27 % of the initial protein amount was retained on the surface of CD-PEI25k or CD-PEI600, regardless of whether the CDs had titratable or non-titratable positive charges on their surface. It was expected that the acidic pH and the high ionic strength of ALF would cause a rapid dissociation of the proteins from the surface of the CDs. These data are consistent with previous results of Rabel et al. who showed that the majority of the corona proteins bounded on iron oxide NPs are detached from the NP surface within the first hour of incubation in ALF medium, with a stabilization of protein

dissociation from 4 h (Rabel et al., 2021). The fact that proteins from the corona can be rapidly degraded in lysosome has also been previously reported in an in vitro study, with a majority of proteins degraded in the lysosome within 8-16 h following NP cell uptake (Bertoli et al., 2016). However, it was also reported that the proteins still present on the surface of the NPs once in the cell and that form the intracellular corona play a major role in the biological effects of NPs (Cai et al., 2022). This will be investigated below.

3.4.2. Evolution of physicochemical properties of CD-T and CD-NT corona proteins under lysosomal conditions

To gain a more detailed understanding of the evolution of the corona formed on CDs after trafficking into the lysosome, proteins adsorbed on the surface of CDs within the initial and the post ALF coronas were then identified and quantified by quantitative proteomic analysis. These proteins were first classified according to their intrinsic physicochemical characteristics, including molecular weight (MW), isoelectric point (pI) and grand Average of Hydropathy (GRAVY) index, which is used to represent the hydrophobicity of the proteins. As shown in Fig. 5a, the MW distribution of the proteins present in the initial coronas was globally homogeneous between the 4 CDs, with a majority of 40-60 kDa proteins. This is in agreement with our previous study which reported a high proportion of intermediate size proteins in the corona of cationic CDs (Arezki et al., 2022a). For PEI25k-based CDs, the post ALF coronas contained a slightly lower proportion of large proteins (> 60 kDa) compared to their respective initial coronas, with a more marked tendency for CD-T than for CD-NT. In line with this, it has been proposed that proteins adsorbed on NPs may be degraded in the lysosome with different kinetics (Ma et al., 2015). In particular, it has been suggested that proteins of low MW would be degraded more slowly than proteins with higher MW (Bertoli et al., 2016). The pI analysis (Fig. 5b) showed that whatever the CDs, the majority of proteins in the initial coronas had a negative net charge at pH 7.4 (i.e., pI < 7). Interestingly, for all CDs, the post ALF coronas contained more proteins with a higher negative charge (i.e., pI < 5). This effect also appeared to be slightly stronger for CD-T than for

CD-NT. These results support the hypothesis that the proteins retained on the surface of CDs under lysosomal conditions are those that are more tightly bound to the surface of CDs by electrostatic interactions. As shown in Fig. 5c, the GRAVY scores of the initial corona proteins were mainly negative, indicating that the initial corona proteins for the 4 CDs are rather hydrophilic. This is to be expected since serum proteins are relatively hydrophilic. Remarkably, the post ALF coronas contained proportionally less hydrophobic proteins (GRAVY index close to 0), especially with regard to CD-T. This suggests that proteins bound to the surface of CDs by hydrophobic interactions are preferentially removed under lysosomal conditions. Thus, for the first time, using proteomic analysis, we characterized the physicochemical properties of the proteins that compose the CD corona after its passage under lysosomal conditions. We showed that the proteins that compose the post ALF corona are different from those of the initial corona in terms of size, charge and hydrophobicity and exhibit the strongest binding to the surface of CDs by electrostatic interactions. The observed changes in the composition of the corona after its passage into the lysosomal fluid are somewhat more pronounced for CD-T than for CD-NT, suggesting that the titratability of the surface charge of CDs may have an impact on the evolution of the corona composition once inside the lysosomal compartment.

3.4.3. Evolution of biological functions of CD-T and CD-NT corona proteins under lysosomal conditions

As seen previously (Fig. 4), the majority (75-95 %) of the initial protein amount was removed from the CD surface under lysosomal conditions. In order to further investigate the consequences of this depletion in terms of protein rearrangement on the surface of the CDs, we analyzed the rank evolution of individual proteins after the passage of CD-protein complexes in lysosomal conditions. Fig. 6 shows the rearrangement of the most abundant proteins which compose the initial and the post ALF corona of the 4 CDs. The rank of each protein in the initial and post ALF corona are shown in italics, with proteins retaining the same rank in the initial and post ALF coronas shown in grey, proteins with downgraded rank in the post ALF corona compared to the initial corona shown in green, and proteins with upgraded rank in the post ALF corona compared to the initial corona shown in pink. We observed

that, for all CDs, only 10-20 % of the proteins retained the same rank in the initial and in the post ALF coronas, while 80-90 % of the corona proteins were rearranged in the post ALF coronas, regardless of whether the CDs had titratable or non-titratable positive charges on their surface. Approximately half of the rearranged proteins were downgraded (i.e., downgraded rank, in green) in the post ALF coronas compared to the initial coronas. For example, ADIPOQ (adiponectin) was downgraded for all 4 CDs in the post ALF coronas, and ALB (albumin) and some apolipoproteins such as APOA1 were downgraded for 3 CDs. In line with our data, these three proteins (ADIPOQ, ALB and APOA1) were described as among the most abundant proteins in the corona of carbon-based NPs (Lu et al., 2019; Machova et al., 2020). In the literature, it has been proposed that a dissociation of the most abundant proteins can be explained by the fact that they are often bound on NP surface by rather low affinity interactions (Nguyen and Lee, 2017). Furthermore, we observed that this dissociation was to the benefit of other proteins. For example, FBLN1, VTN, ITIH3 not only persisted on the surface of the CDs, but also were upgraded (i.e., upgraded rank, in pink) in the post ALF coronas compared to the initial coronas. In addition, some proteins were not present in the initial TOP 20 but were present in the post ALF TOP 20, e.g., HBA (for 4 CDs) and TUBB1 (for 3 CDs). As some of these proteins have specific biological activities, such as ITIH3, which acts as a hyaluronan transporter or as a binding protein with other matrix proteins (Pozzi et al., 2015), it can be assumed that this rearrangement may be associated with biological consequences, which will be discussed later. The dissociation of some proteins from the initial corona followed by the protein rearrangement observed under lysosomal conditions may be related to the physicochemical characteristics of the proteins. Indeed, we have observed previously (Fig. 5) that the proteins retained on the CD surface were in particular proteins with a relatively low pI (i.e., pI < 6). This could be explained by an electrostatic stabilization effect of the most negatively charged proteins on the surface of the CDs when the pH decreases, as opposed to a favored dissociation of proteins with higher pI. Although several interaction mechanisms have been described between proteins and NPs, electrostatic interactions are considered as the most important binding mechanism (Rabel et al., 2021), which our data also indirectly suggest.

Bioinformatics tools such as Panther or STRING systems were next used to analyze the biological functions of the proteins found in the initial and the post ALF coronas. The protein classification according to their molecular function (Fig. 7) revealed that most of the proteins present in the initial corona of the 4 CDs exhibit binding or catalytic activity functions. Notably, these binding and catalytic proteins were particularly retained on the surface of CDs after their passage under lysosomal conditions, and this appeared to be more marked for CD-T than for CD-NT. This result may be important as it has been reported that the interaction of NPs with proteins can lead to protein activation or inactivation in the cellular environment (Walkey et al., 2012). As mentioned above, the physicochemical characteristics of the binding and catalytic proteins could explain their persistence in the corona after its passage into the lysosomal fluid. Indeed, these two groups of proteins were predominantly negatively charged with over half of the proteins with a pI < 6 (Fig. S2). Therefore, they may be preferentially retained on the surface of CDs under lysosomal conditions due to strong electrostatic interactions.

The proteins present in the initial and post ALF coronas of the 4 CDs were then analyzed according to their involvement in KEGG signaling pathways. Fig. 8 shows the main KEGG pathways according to whether they are present in the initial or post ALF coronas of 4 out of 4 CDs (red), 3 out of 4 CDs (orange), 2 out of 4 CDs (yellow), 1 out of 4 CDs (in green), or whether they are not observable (blue). The proteins involved in the pathway of complement and coagulation cascades were present in the initial corona of the 4 CDs, as previously described for the corona of carbon-based NPs (Machova et al., 2020), including CDs (Arezki et al., 2022a). In the literature, complement proteins have in particular been identified as key proteins constituting the corona of NPs, in correlation with NP uptake by immune cells by promoting opsonization (Ju et al., 2020). The initial coronas of the CDs also contained proteins involved in the cholesterol metabolism (4/4 CDs), proteasome (2/4 CDs), phagosome (2/4 CDs), focal adhesion (1/4 CDs) and platelet activation (1/4 CDs) KEGG pathways. Interestingly, all of these pathways were conserved in the post ALF coronas, which means that these groups of proteins persist on the surface of CDs under lysosomal conditions, and therefore may have

intracellular effects. Again, these groups of proteins were distinguished by a predominantly negative charge with an average pI <6 or even around 4, for example for proteins involved in the phagosome and focal adhesion KEGG pathways (Fig. S3). In particular, it is worth noting the persistence of proteins involved in the proteasome system, since the deregulation of this system is involved in a large number of cellular processes such as carcinogenesis or neurodegeneration. In the literature, it has been reported that metallic oxide NPs have the capacity to adsorb some protein subunits of the proteasome and thus act as modulators of the proteasome activity with toxic effects (Falaschetti et al., 2013). Remarkably, due to the dissociation of a large proportion of proteins, we were also able to identify the presence of proteins involved in certain KEGG pathways in the post ALF coronas that were not observable in the initial coronas (Fig. 8). Notably, the KEGG pathways of glycolysis and gluconeogenesis, glucagon signaling pathway or pyruvate metabolism were highlighted in post ALF CD corona. This could impact the intracellular responses induced by CDs by modifying metabolic processes and cellular homeostasis. Indeed, it has recently been reported that the intracellular corona of gold NPs was particularly abundant in glycolysis proteins (e.g., *PKM2*) after escape of the NPs from lysosomes to the cytosol, and that this could disrupt intracellular metabolism (Cai et al., 2022). In addition, we also found that the post ALF CD coronas contained proteins involved in PPAR and PI3K-Akt signaling pathways, which may also modify the intracellular biological responses. For example, the PI3K-Akt-mTOR pathway is a complex signaling pathway involved in carcinogenesis because its deregulation affects cell growth, proliferation or survival. An anticancer effect of selenium NPs through downregulation of the PI3K-Akt-mTOR pathway has been proposed (Wang et al., 2022). But it has also been shown that this anticancer mechanism of NPs is reversed by the presence of a protein corona (Cui et al., 2022). To summarize this section, our data showed that there was a dissociation followed by a subsequent rearrangement of the CD corona proteins after passage of CD-corona complexes under lysosomal conditions, with a persistence of binding proteins, catalytic proteins, and proteins involved in several KEGG pathways such as the proteasome, glycolysis, or PI3k-Akt pathways. These changes were observed for all CDs, whether they carried titratable or non-titratable positive charges

on their surface. But, the persistence of binding and catalytic proteins was more pronounced for CD-T compared to CD-NT, suggesting that the titratability of the surface charge of CDs may have an impact on the selection of corona proteins once in lysosomal compartment. Thus, due to their biological functions, our data suggest that proteins retained on the surface of CDs under lysosomal conditions may contribute to the intracellular effects of the NPs.

4. Conclusions

Our study focused on the complex interaction between the lysosome, the protein corona and the biological effects of CDs. On the one hand, our data confirmed that the lysosome is the subcellular target of cationic CDs, with accumulation of NPs in this organelle, leading to lysosomal swelling, loss of lysosomal integrity, activation of cathepsin B and NLRP3 inflammasome, and ultimately cell death by pyroptosis. We demonstrated also that the titratability of CD cationic surface charges affects these lysosomal key events, as CDs with titratable amine groups induce greater lysosomal dysfunction than CDs with equivalent non-titratable tetraalkylammonium groups. Thus, our data support the hypothesis that the "proton sponge" effect is involved in the biological effects of cationic CDs. On the other hand, using proteomic analysis, we showed that there is a significant dissociation of the initial corona proteins followed by a rearrangement of the remaining proteins when the CDs come into contact with lysosomal conditions, demonstrating an interplay between lysosome and corona in link with CD cationic surface charge titratability. The modulation of the quantity of titratable positive charges on the surface of NPs thus appears to be an interesting approach for further research, in order to better control the intracellular effects of therapeutic NPs.

Figures

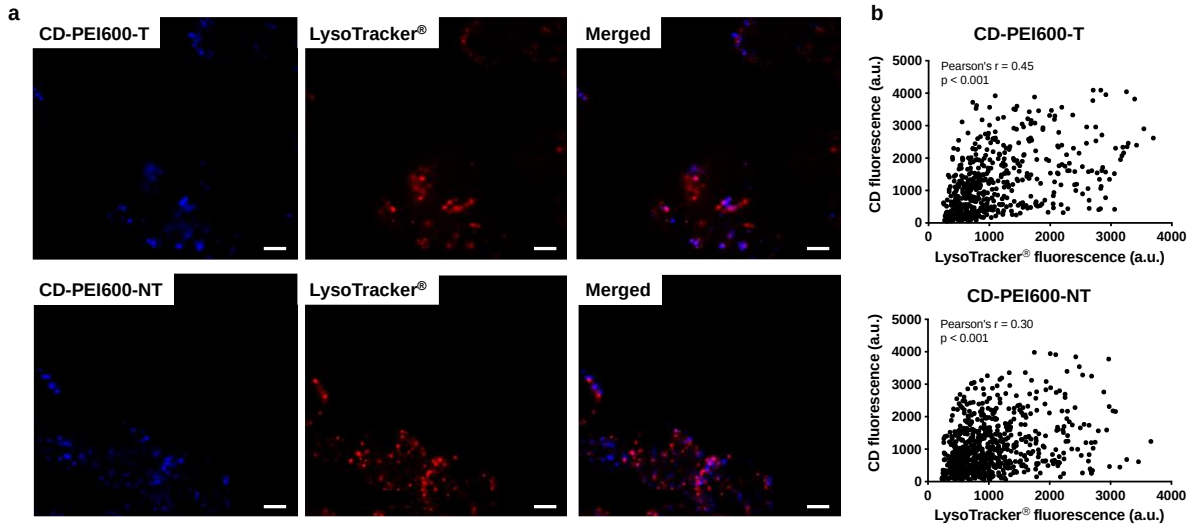

Fig. 1. Colocalization of CDs with lysosomes. Cells were exposed to 12.5 µg/mL of CD-PEI600-T or CD-PEI600-NT for 4 h, and stained with the LysoTracker® Red fluorescent probe before observation by CLSM. a) CLSM pictures of cells. Lysosomes are colored in red and CDs appear in blue (scale bar = 20 µm). b) Quantitative analysis of fluorescence signals associated with CDs and lysosomes, obtained from the analysis of approximately 100 cells per condition.

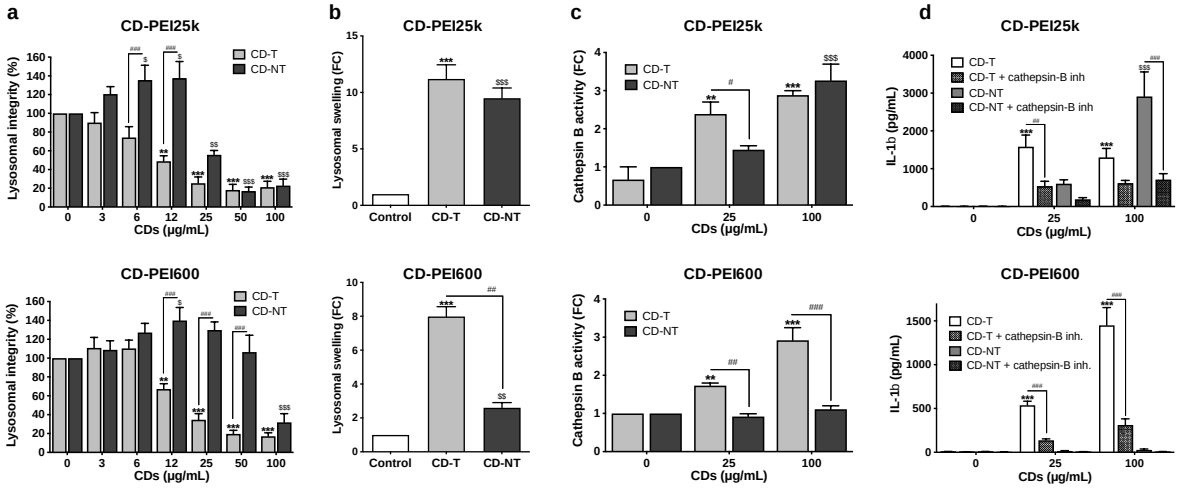

Fig. 2. Lysosomal dysfunction induced by CDs. Cells were exposed to CDs (a: 3-100 µg/mL; b: 25 µg/mL; c: 25 and 100 µg/mL) for 24 h (a and b) or 4 h (c) before lysosomal integrity (a, neutral red), lysosomal swelling (b, LysoTracker® Red DND-99 staining) and cathepsin B activity (c, Magic Red® assay) assessment. Data are means ± SEM of n = 3-6 experiments. Statistical differences at $p < 0.05$ (one symbol), $p < 0.01$ (two symbols) and $p < 0.001$ (three symbols) were determined by ANOVA followed by the Sidak's test (a and c) or Tukey's test (b) when compared to control unexposed cells (asterisks for CD-T or dollar for CD-NT), or to cells exposed to CD-T (hash). d) Cells were pre-incubated or not with CA-074Me (10 µM) for 1.5 h, and then exposed to CDs (25 or 100 µg/mL) for 24 h before quantification of IL-1β secretion in cell culture supernatants. Data are means ± SEM of n = 4-5 experiments. Statistical differences at $p < 0.01$ (two symbols) and $p < 0.001$ (three symbols) were determined by ANOVA followed by the Tukey's test when compared to control unexposed cells (asterisks for CD-T or dollar for CD-NT), or to cells with inhibitor pre-treatment and CD exposure (hash).

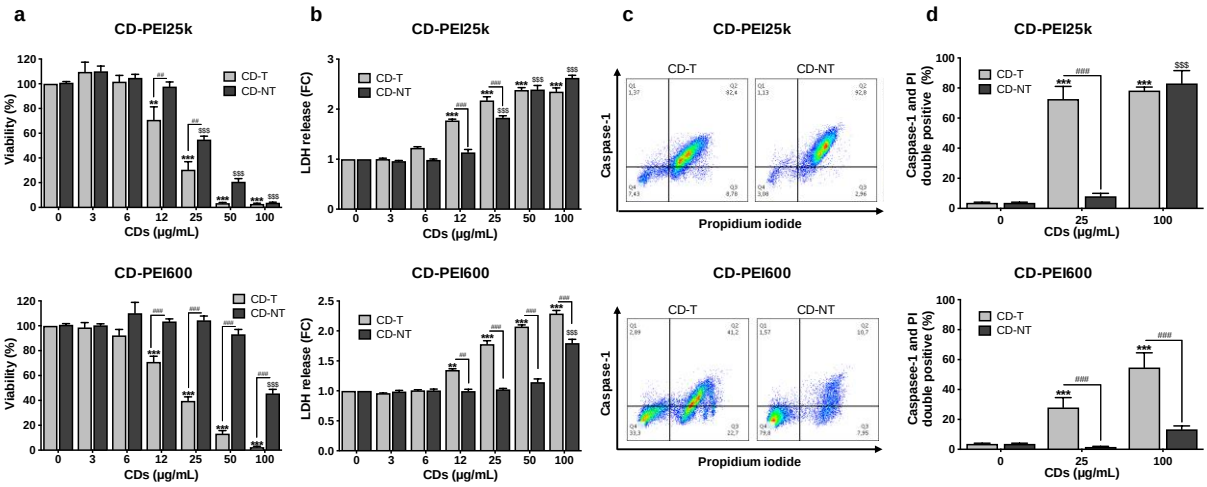

Fig. 3. Cell death mechanism involved in the toxicity of CDs. a) and b) Cells were exposed to increasing concentrations (3-100 µg/mL) of CDs for 24 h before cell viability (a, MTT assay) and necrosis (b, LDH release) measurement. Data are means ± SEM of n = 3-6 experiments. Statistical differences at $p < 0.01$ (two symbols) and $p < 0.001$ (three symbols) were determined by ANOVA followed by the Sidak's test when compared to control unexposed cells (asterisks for CD-T or dollar for CD-NT), or to cells exposed to CD-T (hash). c) and d) Cell pyroptosis induced by CDs. c) Representative flow cytometry chart showing caspase-1 activity as a function of propidium iodide fluorescence in control cells and cells treated with 100 µg/mL of CDs for 4 h. d) Pyroptosis induced by 25 and 100 µg/mL of CDs for 4 h, expressed as percent of double positive cells. Data are means ± SEM of n = 3-6 experiments. Statistical differences at $p < 0.001$ (three symbols) were determined by ANOVA followed by the Sidak's test when compared to control unexposed cells (asterisks for CD-T or dollar for CD-NT), or to cells exposed to CD-T (hash).

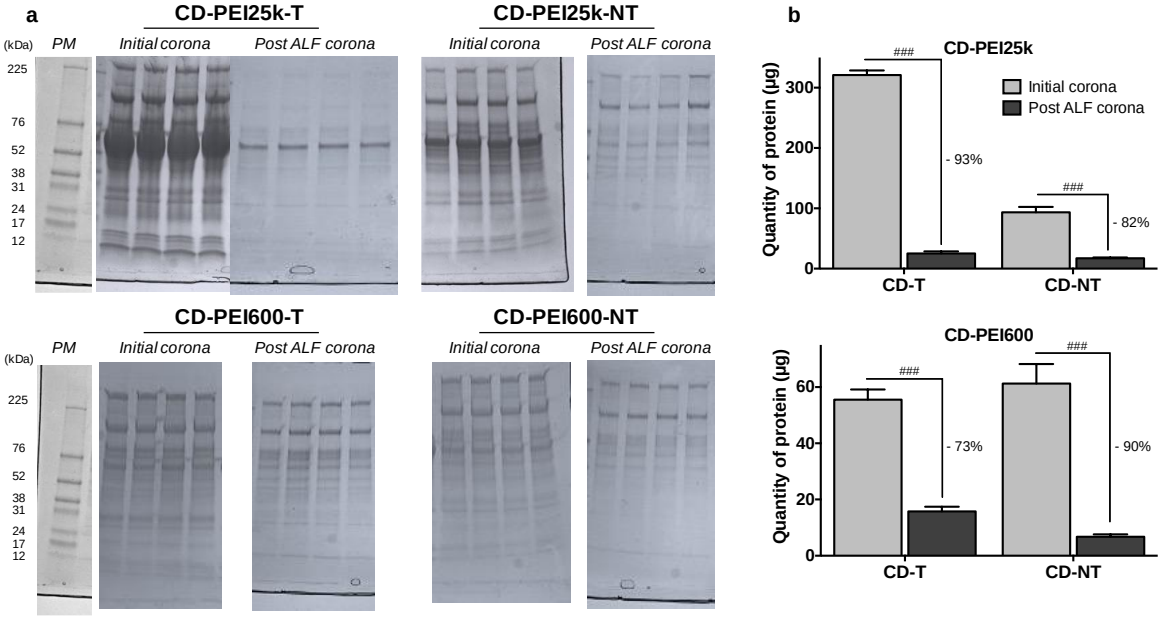

Fig. 4. Characterization of initial and post ALF CD coronas. The CDs were incubated with serum (1 h, 37 °C) to form CD-protein complexes (intial corona), and the latter were then placed in ALF for 4 h to obtain post ALF coronas. The initial and post ALF coronas were characterized by SDS-PAGE analysis (a) and quantification by BCA assay (b) of bound proteins. Data are means ± SEM of n = 4-5 experiments. Statistical differences at $p < 0.001$ (three symbols) were determined by ANOVA followed by the Sidak's test when compared to initial corona.

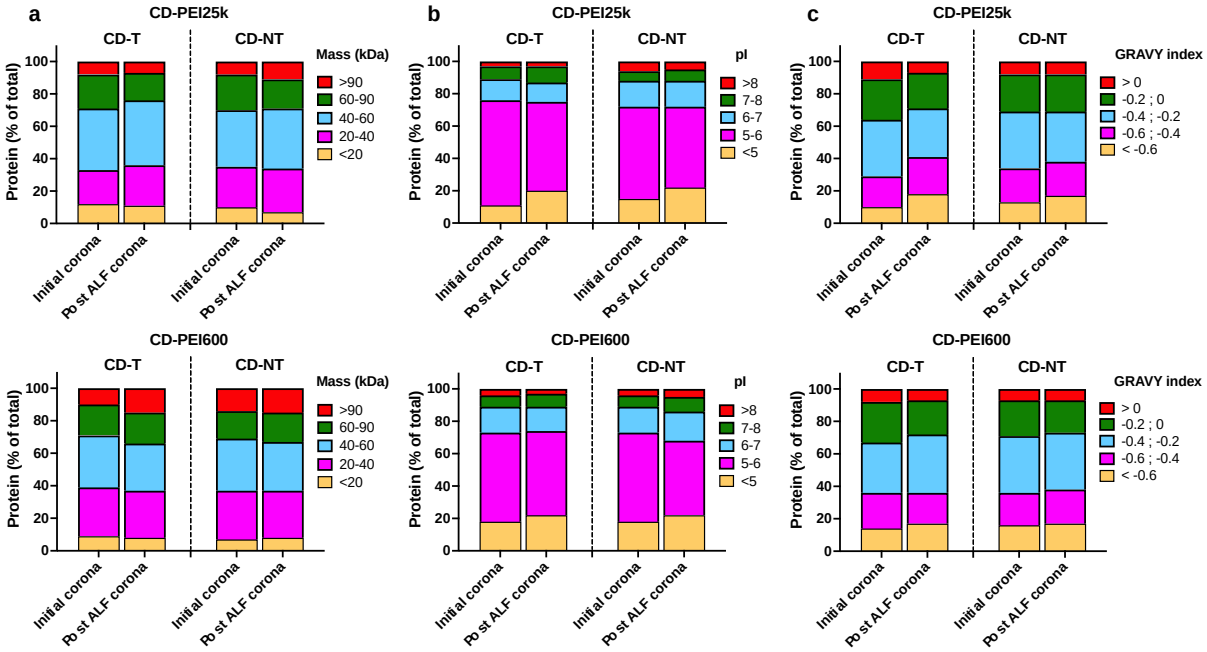

Fig. 5. Physicochemical properties of the proteins identified within the initial and the post ALF CD coronas. Proteins were classified according to their MW (a), pI (b) and GRAVY index (c). Data are expressed as percentage of the total proteins.

CD-PEI25k-T

TOP proteins	Initial corona	Post ALF corona
AHSG	1	1
SERPINA1	2	2
ITIH3	13	13
ALB	9	9
ADIPOQ	3	5
Q9TS74	4	6
APOA1	7	11
C3	10	12
FETUB	14	16
KIF12	15	17
G3N0S9	16	22
SERPINF2	17	18
SERPIND1	18	21
AFP	19	23
VTN	5	3
FBLN1	6	4
SERPINC1	11	10
F2	12	8
P02081	20	14
TUBB1	38	15
HBA	24	19
APOE	22	20

CD-PEI25k-NT

TOP proteins	Initial corona	Post ALF corona
AHSG	1	1
VTN	4	4
C3	7	7
APOA1	13	13
SERPINA1	2	5
ADIPOQ	3	15
Q9TS74	6	10
ALB	9	14
G3N0S9	15	23
FETUB	16	29
SERPIND1	18	19
APOE	19	24
LGALS3BP	20	41
FBLN1	5	3
ITIH3	8	2
F2	10	6
SERPINC1	12	9
KIF12	14	8
P02081	17	12
ITIH2	23	11
HBA	24	17
SERPINF2	21	18
ITIH1	42	20

CD-PEI600-T

TOP proteins	Initial corona	Post ALF corona
C3	7	7
LGALS3BP	15	15
F13A1	19	19
AHSG	1	4
ADIPOQ	2	5
SERPINA1	3	10
G3N0S9	8	12
APOA1	10	16
APOE	12	13
ALB	13	24
FETUB	17	43
Q9TS74	18	28
VTN	4	1
FBLN1	5	2
ITIH3	6	3
KIF12	9	8
F2	11	6
SERPINC1	16	9
P02081	20	11
HBA	34	14
TUBB1	26	17
SERPIND1	23	18
GAPDH	40	20

CD-PEI600-NT

TOP proteins	Initial corona	Post ALF corona
ITIH2	13	13
G3N0S9	15	15
AHSG	1	5
SERPINA1	2	9
ADIPOQ	4	23
C3	7	8
ALB	9	26
LGALS3BP	10	20
Q9TS74	12	39
APOA1	14	21
FETUB	17	74
VTN	3	1
FBLN1	5	2
ITIH3	6	3
KIF12	8	4
SERPINC1	16	6
APOE	18	14
F2	19	10
SERPIND1	20	16
P02081	27	7
HBA	31	11
TUBB1	26	12
F13A1	21	17
CLEC11A	25	19
GAPDH	41	18

Fig. 6. Rearrangement of the TOP most abundant proteins which compose the initial and the post ALF CD coronas. The rank of each protein in the initial and post ALF coronas are shown in italics. Some proteins are in the same rank in the initial and post ALF coronas (grey), some proteins are less abundant in the post ALF corona compared to the initial corona (i.e., downgraded rank, green), and some proteins are more abundant in the post ALF corona compared to the initial corona (i.e., upgraded rank, pink).

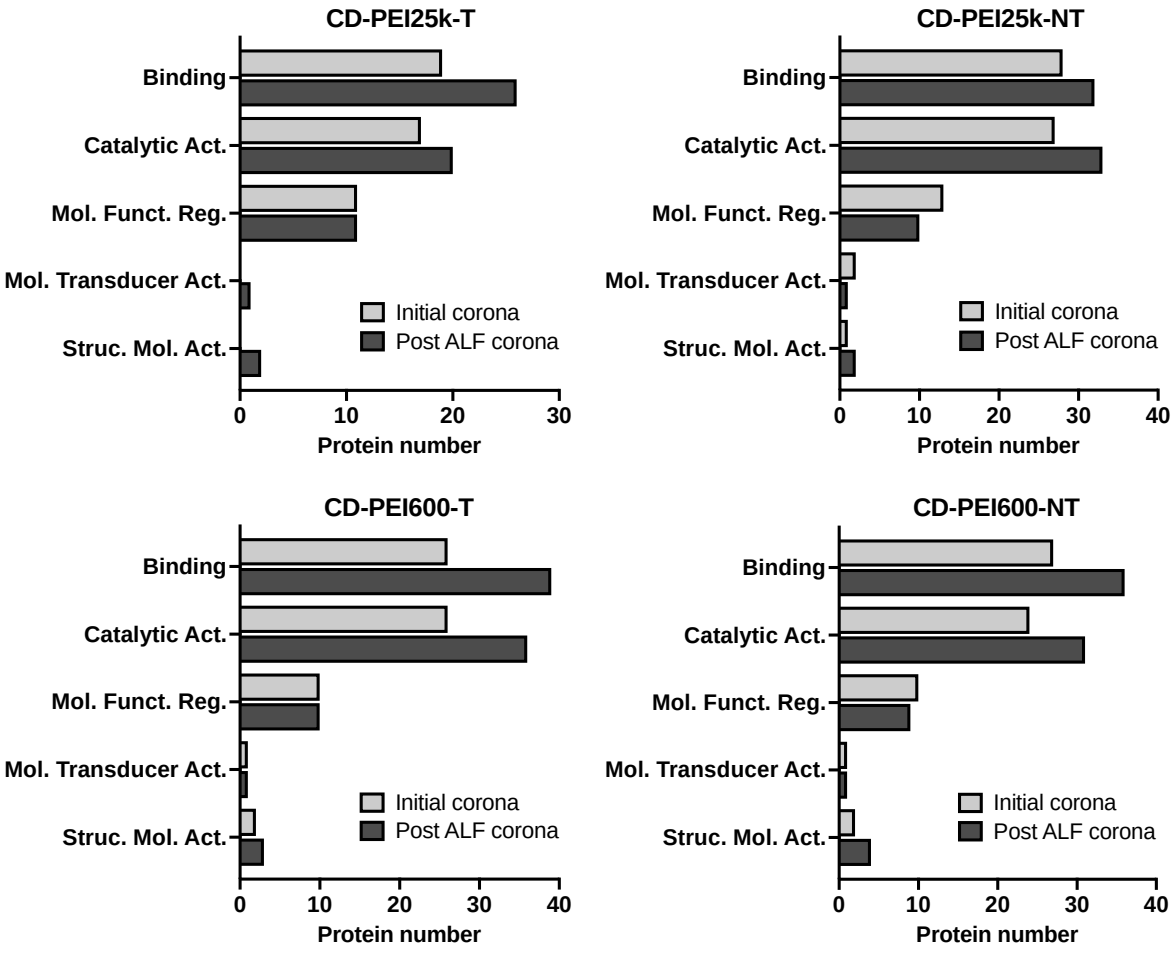

Fig. 7. Biological functions of the proteins identified within the initial and the post ALF CD coronas. Proteins were classified according to their molecular functions.

KEGG Pathways	Initial corona	Post ALF corona
Complement and coagulation cascades		
Cholesterol metabolism		*CD-PEI25k-T; CD-PEI25k-NT; CD-PEI600-T*
Proteasome	*CD-PEI600-T; CD-PEI600-NT*	*CD-PEI25k-NT; CD-PEI600-T; CD-PEI600-NT*
Phagosome	*CD-PEI600-T; CD-PEI600-NT*	
Focal adhesion	*CD-PEI600-NT*	*CD-PEI25k-NT; CD-PEI600-T; CD-PEI600-NT*
Platelet activation	*CD-PEI600-NT*	*CD-PEI25k-NT; CD-PEI600-T; CD-PEI600-NT*
Glycolysis / Gluconeogenesis		*CD-PEI25k-NT; CD-PEI600-T; CD-PEI600-NT*
Pyruvate metabolism		*CD-PEI25k-NT; CD-PEI600-T; CD-PEI600-NT*
Cysteine and methionine metabolism		*CD-PEI25k-NT; CD-PEI600-T*
PPAR signaling pathway		*CD-PEI25k-NT; CD-PEI600-T*
PI3K-Akt signaling pathway		*CD-PEI600-T; CD-PEI600-NT*
Gap junction		*CD-PEI600-T; CD-PEI600-NT*
Tight junction		*CD-PEI600-T; CD-PEI600-NT*
Glucagon signaling pathway		*CD-PEI600-NT*
Biosynthesis of amino acids		*CD-PEI600-T*

4/4 CDs
3/4 CDs
2/4 CDs
1/4 CDs
0/4 CDs

Fig. 8. Analysis of the proteins identified within the initial and the post ALF CD coronas according to their involvement in KEGG signaling pathways. The KEGG pathways are represented according to whether they are present in the initial or post ALF coronas of 4 out of 4 CDs (red), 3 out of 4 CDs (orange), 2 out of 4 CDs (yellow), 1 out of 4 CDs (green), or whether they are not observable (blue).

CRediT authorship contribution statement

Yasmin Arezki: Methodology, Investigation, Formal analysis, Visualization. **Ezeddine Harmouch:** Formal analysis. **François Delalande:** Methodology, Formal analysis. **Mickaël Rapp:** Investigation. **Christine Schaeffer-Reiss:** Methodology, Resources. **Sarah Cianférani:** Resources. **Ophélie Galli:** Investigation. **Luc Lebeau:** Supervision, Writing - Review & Editing. **Françoise Pons:** Supervision, Writing - Review & Editing. **Carole Ronzani:** Conceptualization, Methodology, Formal analysis, Writing - Original Draft, Supervision, Project administration, Funding acquisition.

Acknowledgements

The authors thank Pascal Didier for its help with CLSM (Laboratoire de Bioimagerie et Pathologies, UMR 7021, CNRS-Université de Strasbourg, Illkirch, France), as well as Claudine Ebel and Muriel Koch for their help with FACS experiments (Cytometry platform, IGBMC, Strasbourg).

Funding

This research was supported by the Agence Nationale de la Recherche (ANR, ANR-18-CE34-0005-01), by the Interdisciplinary Thematic Institute 2021-2028 program of the University of Strasbourg, CNRS and Inserm (ANR-10-IDEX-0002 and ANR-20-SFRI-0012) in the frame of the InnoVec Institute, and by the French Proteomic Infrastructure (ProFI, ANR-10-INBS-08-03).

Declaration of Competing Interest

The authors declare that they have no known competing financial interests or personal relationships that could have appeared to influence the work reported in this paper.

Data availability

Data will be made available on request.

References

Arbab, A.S., Wilson, L.B., Ashari, P., Jordan, E.K., Lewis, B.K., Frank, J.A., 2005. A model of lysosomal metabolism of dextran coated superparamagnetic iron oxide (SPIO) nanoparticles: implications for cellular magnetic resonance imaging. NMR Biomed. 18, 383-389. https://doi.org/10.1002/nbm.970.

Arezki, Y., Cornacchia, J., Rapp, M., Lebeau, L., Pons, F., Ronzani, C., 2021. A co-culture model of the human respiratory tract to discriminate the toxicological profile of cationic nanoparticles according to their surface charge density. Toxics 9, 210. https://doi.org/10.3390/toxics9090210.

Arezki, Y., Delalande, F., Schaeffer-Reiss, C., Cianferani, S., Rapp, M., Lebeau, L., Pons, F., Ronzani, C., 2022a. Surface charge influences protein corona, cell uptake and biological effects of carbon dots. Nanoscale 14, 14695-14710. https://doi.org/10.1039/d2nr03611h.

Arezki, Y., Rapp, M., Lebeau, L., Ronzani, C., Pons, F., 2022b. Cationic carbon nanoparticles induce inflammasome-dependent pyroptosis in macrophages via lysosomal dysfunction. Front. Toxicol. 4, 925399. https://doi.org/10.3389/ftox.2022.925399.

Beeston, M.P., van Elteren, J.T., Selih, V.S., Fairhurst, R., 2010. Characterization of artificially generated PbS aerosols and their use within a respiratory bioaccessibility test. Analyst 135, 351-357. https://doi.org/10.1039/b910429a.

Behr, J.P., 1997. The proton sponge: A trick to enter cells the viruses did not exploit. Chimia 51, 34-36. https://doi.org/10.2533/chimia.1997.34

Bertoli, F., Garry, D., Monopoli, M.P., Salvati, A., Dawson, K.A., 2016. The intracellular destiny of the protein corona: A study on its cellular internalization and evolution. ACS Nano 10, 10471-10479. https://doi.org/10.1021/acsnano.6b06411.

Boya, P., Kroemer, G., 2008. Lysosomal membrane permeabilization in cell death. Oncogene 27, 6434-6451. https://doi.org/10.1038/onc.2008.310.

Cai, R., Ren, J.Y., Guo, M.Y., Wei, T.T., Liu, Y., Xie, C.Y., Zhang, P., Guo, Z.L., Chetwynd, A.J., Ke, P.C., Lynch, I., Chen, C.Y., 2022. Dynamic intracellular exchange of nanomaterials' protein corona perturbs proteostasis and remodels cell metabolism. Proc. Natl. Acad. Sci. USA. 119, e2200363119. https://doi.org/10.1073/pnas.2200363119.

Canton, I., Battaglia, G., 2012. Endocytosis at the nanoscale. Chem. Soc. Rev. 41, 2718-2739. https://doi.org/10.1039/c2cs15309b.

Chanput, W., Mes, J.J., Wichers, H.J., 2014. THP-1 cell line: An in vitro cell model for immune modulation approach. Int. Immunopharmacol. 23, 37-45. https://doi.org/10.1016/j.intimp.2014.08.002.

Claudel, M., Fan, J.H., Rapp, M., Pons, F., Lebeau, L., 2019. Influence of carbonization conditions on luminescence and gene delivery properties of nitrogen-doped carbon dots. RSC Adv. 9, 3493. https://doi.org/10.1039/C8RA09651A.

Cui, L.S., Quagliarini, E., Xiao, S.Y., Giulimondi, F., Renzi, S., Digiacomo, L., Caracciolo, G., Wang, J.B., Amici, A., Marchini, C., Pozzi, D., 2022. The protein corona reduces the anticancer effect of graphene oxide in HER-2-positive cancer cells. Nanoscale Adv. 4, 4009-4015. https://doi.org/10.1039/d2na00308b.

Ding, L., Yao, C.J., Yin, X.F., Li, C.C., Huang, Y.A., Wu, M., Wang, B., Guo, X.Y., Wang, Y.L., Wu, M.H., 2018. Size, shape, and protein corona determine cellular uptake and removal mechanisms of gold nanoparticles. Small 14, 1801451. https://doi.org/10.1002/smll.201801451.

Du, J.J., Xu, N., Fan, J.L., Sun, W., Peng, X.J., 2019. Carbon dots for in vivo bioimaging and theranostics. Small 15, 1805087. https://doi.org/10.1002/smll.201805087.

E, S., Mao, Q.X., Yuan, X.L., Kong, X.L., Chen, X.W., Wang, J.H., 2018. Targeted imaging of the lysosome and endoplasmic reticulum and their pH monitoring with surface regulated carbon dots. Nanoscale 10, 12788-12796. https://doi.org/10.1039/c8nr03453b.

Faizullin, B., Gubaidullin, A., Gerasimova, T., Kashnik, I., Brylev, K., Kholin, K., Nizameev, I., Voloshina, A., Sibgatullina, G., Samigullin, D., Petrov, K., Musina, E., Karasik, A., Mustafina, A., 2022. "Proton sponge" effect and apoptotic cell death mechanism of Agx-Re6 nanocrystallites derived from the assembly of [{Re6S8}(OH)6-n(H2O)n]n-4 with Ag+ ions. Colloid. Surface A. 648, 129312. https://doi.org/10.1016/j.colsurfa.2022.129312.

Falaschetti, C.A., Paunesku, T., Kurepa, J., Nanavati, D., Chou, S.S., De, M., Song, M., Jang, J.T., Wu, A.G., Dravid, V.P., Cheon, J., Smalle, J., Woloschak, G.E., 2013. Negatively charged metal oxide nanoparticles interact with the 20S proteasome and differentially modulate its biologic functional effects. ACS Nano 7, 7759-7772. https://doi.org/10.1021/nn402416h.

Fan, J.H., Claudel, M., Ronzani, C., Arezki, Y., Lebeau, L., Pons, F., 2019. Physicochemical characteristics that affect carbon dot safety: Lessons from a comprehensive study on a nanoparticle library. Int. J. Pharmaceut. 569, 118521. https://doi.org/10.1016/j.ijpharm.2019.118521.

Feng, T., Ai, X.Z., An, G.H., Yang, P.P., Zhao, Y.L., 2016. Charge-convertible carbon dots for imaging guided drug delivery with enhanced in vivo cancer therapeutic efficiency. ACS Nano 10, 4410-4420. https://doi.org/10.1021/acsnano.6b00043.

Ghosal, K., Ghosh, A., 2019. Carbon dots: The next generation platform for biomedical applications. Mat. Sci. Eng. C-Mater. 96, 887-903. https://doi.org/10.1016/j.msec.2018.11.060.

Himaja, A.L., Karthik, P.S., Singh, S.P., 2015. Carbon dots: the newest member of the carbon nanomaterials family. Chem. Rec. 15, 595-615. https://doi.org/10.1002/tcr.201402090.

Huang, D.P., Zhou, H.F., Wu, Y.Q., Wang, T., Sun, L.L., Gao, P., Sun, Y.Z., Huang, H.N., Zhou, G.J., Hu, J.F., 2019. Bottom-up synthesis and structural design strategy for graphene quantum dots with tunable emission to the near infrared region. Carbon 142, 673-684. https://doi.org/10.1016/j.carbon.2018.10.047.

Huhn, D., Kantner, K., Geidel, C., Brandholt, S., De Cock, I., Soenen, S.J., Rivera Gil, P., Montenegro, J.M., Braeckmans, K., Mullen, K., Nienhaus, G.U., Klapper, M., Parak, W.J., 2013. Polymer-coated nanoparticles interacting with proteins and cells: focusing on the sign of the net charge. ACS Nano 7, 3253-3263. https://doi.org/10.1021/nn3059295.

Ju, Y., Kelly, H.G., Dagley, L.F., Reynaldi, A., Schlub, T.E., Spall, S.K., Bell, C.A., Cui, J.W., Mitchell, A.J., Lin, Z.X., Wheatley, A.K., Thurecht, K.J., Davenport, M.P., Webb, A.I., Caruso, F., Kent, S.J., 2020. Person-specific biomolecular coronas modulate nanoparticle interactions with immune cells in human blood. ACS Nano 14, 15723-15737. https://doi.org/10.1021/acsnano.0c06679.

Keshavan, S., Gupta, G., Martin, S., Fadeel, B., 2021. Multi-walled carbon nanotubes trigger lysosome-dependent cell death (pyroptosis) in macrophages but not in neutrophils. Nanotoxicology 15, 1125-1150. https://doi.org/10.1080/17435390.2021.1988171.

Kirkegaard, T., Jaattela, M., 2009. Lysosomal involvement in cell death and cancer. Biochim. Biophys. Acta. 1793, 746-754. https://doi.org/10.1016/j.bbamcr.2008.09.008.

Lee, G.Y., Lo, P.Y., Cho, E.C., Zheng, J.H., Li, M., Huang, J.H., Lee, K.C., 2022. Integration of PEG and PEI with graphene quantum dots to fabricate pH-responsive nanostars for colon cancer suppression in vitro and in vivo. Flatchem. 31, 100320. https://doi.org/10.1016/j.flatc.2021.100320.

Lenz, C., Dihazi, H., 2016. Introduction to proteomics technologies. Methods Mol. Biol. 1362, 3-27. https://doi.org/10.1007/978-1-4939-3106-4_1.

Li, M.H., Gao, X.L., Lin, C., Shen, A.J., Luo, J., Ji, Q.Q., Wu, J.Q., Wang, P.J., 2021. An intelligent responsive macrophage cell membrane-camouflaged mesoporous silicon nanorod drug delivery system for precise targeted therapy of tumors. J. Nanobiotechnol. 19, 336. https://doi.org/10.1186/s12951-021-01082-1.

Liu, K.J., Song, Y.K., Tan, M.Q., 2020. Toxicity alleviation of carbon dots from roast beef after the formation of protein coronas with human serum albumin. J. Agr. Food Chem. 68, 9789-9795. https://doi.org/10.1021/acs.jafc.0c03499.

Lu, X., Xu, P.P., Ding, H.M., Yu, Y.S., Huo, D., Ma, Y.Q., 2019. Tailoring the component of protein corona via simple chemistry. Nat. Commun. 10, 4520. https://doi.org/10.1038/s41467-019-12470-5.

Lynch, I., Salvati, A., Dawson, K.A., 2009. Protein-nanoparticle interactions: What does the cell see? Nat. Nanotechnol. 4, 546-547. https://doi.org/10.1038/nnano.2009.248.

Ma, Z.F., Bai, J., Jiang, X.E., 2015. Monitoring of the enzymatic degradation of protein corona and evaluating the accompanying cytotoxicity of nanoparticles. ACS Appl. Mater. Inter. 7, 17614-17622. https://doi.org/10.1021/acsami.5b05744.

Machova, I., Hubalek, M., Belinova, T., Fucikova, A., Stehlik, S., Rezek, B., Kalbacova, M.H., 2020. The bio-chemically selective interaction of hydrogenated and oxidized ultra-small nanodiamonds with proteins and cells. Carbon 162, 650-661. https://doi.org/10.1016/j.carbon.2020.02.061.

Milosevic, A., Bourquin, J., Burnand, D., Lemal, P., Crippa, F., Monnier, C.A., Rodriguez-Lorenzo, L., Petri-Fink, A., Rothen-Rutishauser, B., 2019. Artificial lysosomal platform to study nanoparticle long-term stability. Chimia 73, 55-58. https://doi.org/10.2533/chimia.2019.55.

Milosevic, A.M., Rodriguez-Lorenzo, L., Balog, S., Monnier, C.A., Petri-Fink, A., Rothen-Rutishauser, B., 2017. Assessing the stability of fluorescently encoded nanoparticles in lysosomes by using complementary methods. Angew Chem. Int. Ed. Engl. 56, 13382-13386. https://doi.org/10.1002/anie.201705422.

Nakayama, M., 2018. Macrophage recognition of crystals and nanoparticles. Front. Immunol 9, 103. https://doi.org/10.3389/fimmu.2018.00103.

Nguyen, V.H., Lee, B.J., 2017. Protein corona: a new approach for nanomedicine design. Int. J. Nanomed. 12, 3137-3151. https://doi.org/10.2147/ljn.S129300.

Peng, Y.Y., Cong, Y.Y., Lei, Y.Z., Sun, F.W., Xu, M.H., Zhang, J.Z., Fang, L., Hong, H., Cai, T., 2022. Transforming passive into active: multimodal pheophytin-based carbon dots customize protein corona to target metastatic breast cancer. Adv. Healthc. Mater. 11, e2102270. https://doi.org/10.1002/adhm.202102270.

Perez-Riverol, Y., Bai, J.W., Bandla, C., Garcia-Seisdedos, D., Hewapathirana, S., Kamatchinathan, S., Kundu, D.J., Prakash, A., Frericks-Zipper, A., Eisenacher, M., Walzer, M., Wang, S.B., Brazma, A., Vizcaino, J.A., 2022. The PRIDE database resources in 2022: a hub for mass spectrometry-based proteomics evidences. Nucleic Acids Res. 50, 543-552. https://doi.org/10.1093/nar/gkab1038.

Pierrat, P., Wang, R.R., Kereselidze, D., Lux, M., Didier, P., Kichler, A., Pons, F., Lebeau, L., 2015. Efficient in vitro and in vivo pulmonary delivery of nucleic acid by carbon dot-based nanocarriers. Biomaterials 51, 290-302. https://doi.org/10.1016/j.biomaterials.2015.02.017.

Pozzi, D., Caracciolo, G., Digiacomo, L., Colapicchioni, V., Palchetti, S., Capriotti, A.L., Cavaliere, C., Chiozzi, R.Z., Puglisi, A., Lagana, A., 2015. The biomolecular corona of nanoparticles in circulating biological media. Nanoscale 7, 13958-13966. https://doi.org/10.1039/c5nr03701h.

Rabel, M., Warncke, P., Gruttner, C., Bergemann, C., Kurland, H.D., Muller, R., Dugandzic, V., Thamm, J., Muller, F.A., Popp, J., Cialla-May, D., Fischer, D., 2019. Simulation of the long-term fate of superparamagnetic iron oxide-based nanoparticles using simulated biological fluids. Nanomedicine (Lond.) 14, 1681-1706. https://doi.org/10.2217/nnm-2018-0382.

Rabel, M., Warncke, P., Thurmer, M., Gruttner, C., Bergemann, C., Kurland, H.D., Muller, F.A., Koeberle, A., Fischer, D., 2021. The differences of the impact of a lipid and protein corona on the colloidal stability, toxicity, and degradation behavior of iron oxide nanoparticles. Nanoscale 13, 9415-9435. https://doi.org/10.1039/d0nr09053k.

Reisetter, A.C., Stebounova, L.V., Baltrusaitis, J., Powers, L., Gupta, A., Grassian, V.H., Monick, M.M., 2011. Induction of inflammasome-dependent pyroptosis by carbon black nanoparticles. J. Biol. Chem. 286, 21844-21852. https://doi.org/10.1074/jbc.M111.238519.

Repnik, U., Hafner Cesen, M., Turk, B., 2014. Lysosomal membrane permeabilization in cell death: concepts and challenges. Mitochondrion 19 Pt A, 49-57. https://doi.org/10.1016/j.mito.2014.06.006.

Ronzani, C., Van Belle, C., Didier, P., Spiegelhalter, C., Pierrat, P., Lebeau, L., Pons, F., 2019. Lysosome mediates toxicological effects of polyethyleneimine-based cationic carbon dots. J. Nanopart. Res. 21, 4. https://doi.org/10.1007/s11051-018-4438-5.

Sahay, G., Alakhova, D.Y., Kabanov, A.V., 2010. Endocytosis of nanomedicines. J. Control Release 145, 182-195. https://doi.org/10.1016/j.jconrel.2010.01.036.

Sciortino, A., Cannizzo, A., Messina, F., 2018. Carbon nanodots: A review-from the current understanding of the fundamental photophysics to the full control of the optical response. C-J. Carbon Res. 4, 67. https://doi.org/10.3390/c4040067.

Settembre, C., Fraldi, A., Medina, D.L., Ballabio, A., 2013. Signals from the lysosome: a control centre for cellular clearance and energy metabolism. Nat. Rev. Mol. Cell. Biol. 14, 283-296. https://doi.org/10.1038/nrm3565.

Song, Y.K., Wang, H.T., Zhang, L.J., Lai, B., Liu, K.J., Tan, M.Q., 2020. Protein corona formation of human serum albumin with carbon quantum dots from roast salmon. Food Funct. 11, 2358-2367. https://doi.org/10.1039/c9fo02967b.

Stepien, G., Moros, M., Perez-Hernandez, M., Monge, M., Gutierrez, L., Fratila, R.M., Heras, M.D., Guillen, S.M., Lanzarote, J.J.P., Solans, C., Pardo, J., de la Fuente, J.M., 2018. Effect of surface chemistry and associated protein corona on the long-term biodegradation of iron oxide nanoparticles in vivo. ACS Appl. Mater. Inter. 10, 4548-4560. https://doi.org/10.1021/acsami.7b18648.

Stern, S.T., Adiseshaiah, P.P., Crist, R.M., 2012. Autophagy and lysosomal dysfunction as emerging mechanisms of nanomaterial toxicity. Part. Fibre Toxicol. 9, 20. https://doi.org/10.1186/1743-8977-9-20.

Svadlakova, T., Hubatka, F., Knotigova, P.T., Kulich, P., Masek, J., Kotoucek, J., Macak, J., Motola, M., Kalbac, M., Kolackova, M., Vankova, R., Vicherkova, P., Malkova, A., Simeckova, P., Volkov, Y., Prina-Mello, A., Kratochvilova, I., Fiala, Z., Raska, M., Krejsek, J., Turanek, J., 2020. Proinflammatory effect of carbon-based nanomaterials: In vitro study on stimulation of inflammasome NLRP3 via destabilisation of lysosomes. Nanomaterials-Basel 10, 481. https://doi/org/10.3390/nano10030418.

Tahara, Y., Nakamura, M., Yang, M., Zhang, M., Iijima, S., Yudasaka, M., 2012. Lysosomal membrane destabilization induced by high accumulation of single-walled carbon nanohorns in murine macrophage RAW 264.7. Biomaterials 33, 2762-2769. https://doi.org/10.1016/j.biomaterials.2011.12.023.

Tan, Y., Zhu, X.Y., Wu, D., Song, E.Q., Song, Y., 2020. Compromised autophagic effect of polystyrene nanoplastics mediated by protein corona was recovered after lysosomal degradation of corona. Environ. Sci. Technol. 54, 11485-11493. https://doi.org/10.1021/acs.est.0c04097.

Truskewycz, A., Yin, H., Halberg, N., Lai, D.T.H., Ball, A.S., Truong, V.K., Rybicka, A.M., Cole, I., 2022. Carbon dot therapeutic platforms: administration, distribution, metabolism, excretion, toxicity, and therapeutic potential. Small 18, 2106342. https://doi.org/ 10.1002/smll.202106342.

Vermeulen, L.M.P., Brans, T., Samal, S.K., Dubruel, P., Demeester, J., De Smedt, S.C., Remaut, K., Braeckmans, K., 2018. Endosomal size and membrane leakiness influence proton sponge-based rupture of endosomal vesicles. ACS Nano 12, 2332-2345. https://doi.org/10.1021/acsnano.7b07583.

Walkey, C.D., Olsen, J.B., Guo, H.B., Emili, A., Chan, W.C.W., 2012. Nanoparticle size and surface chemistry determine serum protein adsorption and macrophage uptake. J. Am. Chem. Soc. 134, 2139-2147. https://doi.org/10.1021/ja2084338.

Wang, C., Chen, B.B., He, M., Hu, B., 2021. Composition of intracellular protein corona around nanoparticles during internalization. ACS Nano 15, 3108-3122. https://doi.org/10.1021/acsnano.0c09649.

Wang, F., Bexiga, M.G., Anguissola, S., Boya, P., Simpson, J.C., Salvati, A., Dawson, K.A., 2013a. Time resolved study of cell death mechanisms induced by amine-modified polystyrene nanoparticles. Nanoscale 5, 10868-10876. https://doi.org/10.1039/c3nr03249c.

Wang, F., Gomez-Sintes, R., Boya, P., 2018. Lysosomal membrane permeabilization and cell death. Traffic 19, 918-931. https://doi.org/10.1111/tra.12613.

Wang, F.J., Yu, L., Monopoli, M.P., Sandin, P., Mahon, E., Salvati, A., Dawson, K.A., 2013b. The biomolecular corona is retained during nanoparticle uptake and protects the cells from the damage induced by cationic nanoparticles until degraded in the lysosomes. Nanomed-Nanotechnol. 9, 1159-1168. https://doi.org/10.1016/j.nano.2013.04.010.

Wang, R.B., Ha, K.Y., Dhandapani, S., Kim, Y.J., 2022. Biologically synthesized black ginger-selenium nanoparticle induces apoptosis and autophagy of AGS gastric cancer cells by suppressing the PI3K/Akt/mTOR signaling pathway. J. Nanobiotechnol. 20, 441. https://doi.org/10.1186/s12951-022-01576-6.

Wang, S.Y., Ma, J., Guo, S., Huang, Y.Y., Cao, Y., 2020. Transcriptomic analysis revealed that multi-walled carbon nanotubes diameter-dependently induced pyroptosis in THP-1 macrophages. Nanoimpact 20, 100270. https://doi.org/10.1016/j.impact.2020.100270.

Weiss, M., Fan, J.H., Claudel, M., Sonntag, T., Didier, P., Ronzani, C., Lebeau, L., Pons, F., 2021. Density of surface charge is a more predictive factor of the toxicity of cationic carbon nanoparticles than zeta potential. J. Nanobiotechnol. 19, 5. https://doi.org/10.1186/s12951-020-00747-7.

Wu, L.L., Li, X.L., Ling, Y.F., Huang, C.S., Jia, N.Q., 2017. Morpholine derivative-functionalized carbon dots-based fluorescent probe for highly selective lysosomal imaging in living cells. ACS Appl. Mater. Inter. 9, 28222-28232. https://doi.org/10.1021/acsami.7b08148.

Wu, Y., Song, X., Wang, N., Cong, S., Zhao, X., Rai, R., Tan, M., 2020. Carbon dots from roasted chicken accumulate in lysosomes and induce lysosome-dependent cell death. Food Funct. 11, 10105-10113. https://doi.org/10.1039/d0fo02144j.

Xia, T., Kovochich, M., Liong, M., Zink, J.I., Nel, A.E., 2008. Cationic polystyrene nanosphere toxicity depends on cell-specific endocytic and mitochondrial injury pathways. ACS Nano 2, 85-96. https://doi.org/10.1021/nn700256c.

Xu, X.Y., Ray, R., Gu, Y.L., Ploehn, H.J., Gearheart, L., Raker, K., Scrivens, W.A., 2004. Electrophoretic analysis and purification of fluorescent single-walled carbon nanotube fragments. J. Am. Chem. Soc. 126, 12736-12737. https://doi.org/10.1021/ja040082h.